JOURNAL OF VIROLOGY, Oct. 2006, p. 9465–9480 Vol. 80, No. 19
0022-538X/06/$08.00+0 doi:10.1128/JVI.01049-06

Human ESCRT-II Complex and Its Role in Human Immunodeficiency Virus Type 1 Release†

Charles Langelier,[1] Uta K. von Schwedler,[1] Robert D. Fisher,[1] Ivana De Domenico,[2] Paul L. White,[1] Christopher P. Hill,[1] Jerry Kaplan,[2] Diane Ward,[2] and Wesley I. Sundquist[1]*

Departments of Biochemistry[1] and Pathology,[2] University of Utah, Salt Lake City, Utah 84112

Received 22 May 2006/Accepted 8 July 2006

The budding of many enveloped RNA viruses, including human immunodeficiency virus type 1 (HIV-1), requires some of the same cellular machinery as vesicle formation at the multivesicular body (MVB). In *Saccharomyces cerevisiae*, the ESCRT-II complex performs a central role in MVB protein sorting and vesicle formation, as it is recruited by the upstream ESCRT-I complex and nucleates assembly of the downstream ESCRT-III complex. Here, we report that the three subunits of human ESCRT-II, EAP20, EAP30, and EAP45, have a number of properties in common with their yeast orthologs. Specifically, EAP45 bound ubiquitin via its N-terminal GRAM-like ubiquitin-binding in EAP45 (GLUE) domain, both EAP45 and EAP30 bound the C-terminal domain of TSG101/ESCRT-I, and EAP20 bound the N-terminal half of CHMP6/ESCRT-III. Consistent with its expected role in MVB vesicle formation, (i) human ESCRT-II localized to endosomal membranes in a VPS4-dependent fashion and (ii) depletion of EAP20/ESCRT-II and CHMP6/ESCRT-III inhibited lysosomal targeting and downregulation of the epidermal growth factor receptor, albeit to a lesser extent than depletion of TSG101/ESCRT-I. Nevertheless, HIV-1 release and infectivity were not reduced by efficient small interfering RNA depletion of EAP20/ESCRT-II or CHMP6/ESCRT-III. These observations indicate that there are probably multiple pathways for protein sorting/MVB vesicle formation in human cells and that HIV-1 does not utilize an ESCRT-II-dependent pathway to leave the cell.

Enveloped RNA viruses like human immunodeficiency virus (HIV) acquire lipid bilayers and exit infected cells by budding through limiting membranes. The process of HIV budding shares a number of similarities with the cellular process of vesicle formation at the multivesicular body (MVB) (reviewed in references 2, 14, 25, 26, 33, 40, and 51). MVB vesicles and HIV virions both bud away from the cytoplasm (58) and share the following mechanistic similarities: (i) a requirement for ubiquitin (Ub) in formation and cargo incorporation (reviewed in references 40 and 81), (ii) recruitment and utilization of the cellular ESCRT-I complex (6, 15, 19, 22, 47, 48, 52, 70, 79), and (iii) a requirement for ESCRT-III, LIP5, and VPS4 ATPase activities (22, 46, 69, 83, 85). In spite of these similarities, however, MVB biogenesis and viral budding ultimately create different vesicles, and it is therefore of interest to determine the precise relationship between the two processes.

Genetic screens in *Saccharomyces cerevisiae* defined the basic machinery of MVB vesicle formation and identified 17 soluble yeast proteins that are essential for MVB biogenesis (the "class E" proteins) (40, 59). Complementary biochemical analyses revealed that MVB vesicle formation proceeds through an ordered pathway in which a series of soluble class E complexes, termed ESCRT-I (39), ESCRT-II (4), and ESCRT-III (3), are sequentially recruited to endosomal membranes, where they function in vesicle formation (Fig. 1A). Although the processes of vesicle formation and cargo incorporation are not yet understood in mechanistic detail, ESCRT-I and -II appear to function primarily as adaptors that recognize protein cargoes and help recruit ESCRT-III, which in turn appears to function more directly in protein sorting and vesicle formation.

As the central complex in the yeast ESCRT pathway, ESCRT-II bridges ESCRT-I and ESCRT-III and also interacts with ubiquitylated cargoes. As shown in Fig. 1B, crystal structures of the yeast ESCRT-II core (30, 74) have revealed that the yeast ESCRT-II complex contains two copies of Vps25p (EAP20) that bind asymmetrically to single copies of Vps22p (EAP30) and Vps36p (EAP45) (human protein names are provided in parentheses for reference). The two Vps25p (EAP20) proteins project away from the Vps22p-Vps36p dimer, so that the overall complex assumes a trilobed "Y" shape. The three ESCRT-II subunits are related structurally, as each contains two copies of the winged-helix (WH) protein motif. Two of the proteins also contain N-terminal extensions: Vps22p (EAP30) has an extended helix (Fig. 1B), and Vps36p (EAP45) contains a linker and an N-terminal GRAM-like ubiquitin-binding in EAP45 (GLUE) domain (not present in the core structure). Structural and biochemical analyses of the Vps36p GLUE domain have shown that it is a split PH domain that binds phosphatidylinositol phosphates, particularly PI(3)P (67, 73). An extended insert within the GLUE domain contains two Npl4 zinc fingers (NZF), which are small globular zinc binding modules that mediate protein-protein interactions (49). The first, NZF-N, binds Vps28p (ESCRT-I) and helps recruit ESCRT-II to the endosomal membrane (73), whereas the second, NZF-C, binds ubiquitin and is required for efficient sorting of ubiquitylated cargoes (1).

The human and yeast ESCRT-II complexes are likely to be related structurally, because mammalian ESCRT-II can be iso-

* Corresponding author. Mailing address: Department of Biochemistry, 15 N. Medical Drive East, Room 4100, University of Utah School of Medicine, Salt Lake City, UT 84112-5650. Phone: (801) 585-5402. Fax: (801) 581-7959. E-mail: wes@biochem.utah.edu.

† Supplemental material for this article may be found at http://jvi.asm.org.

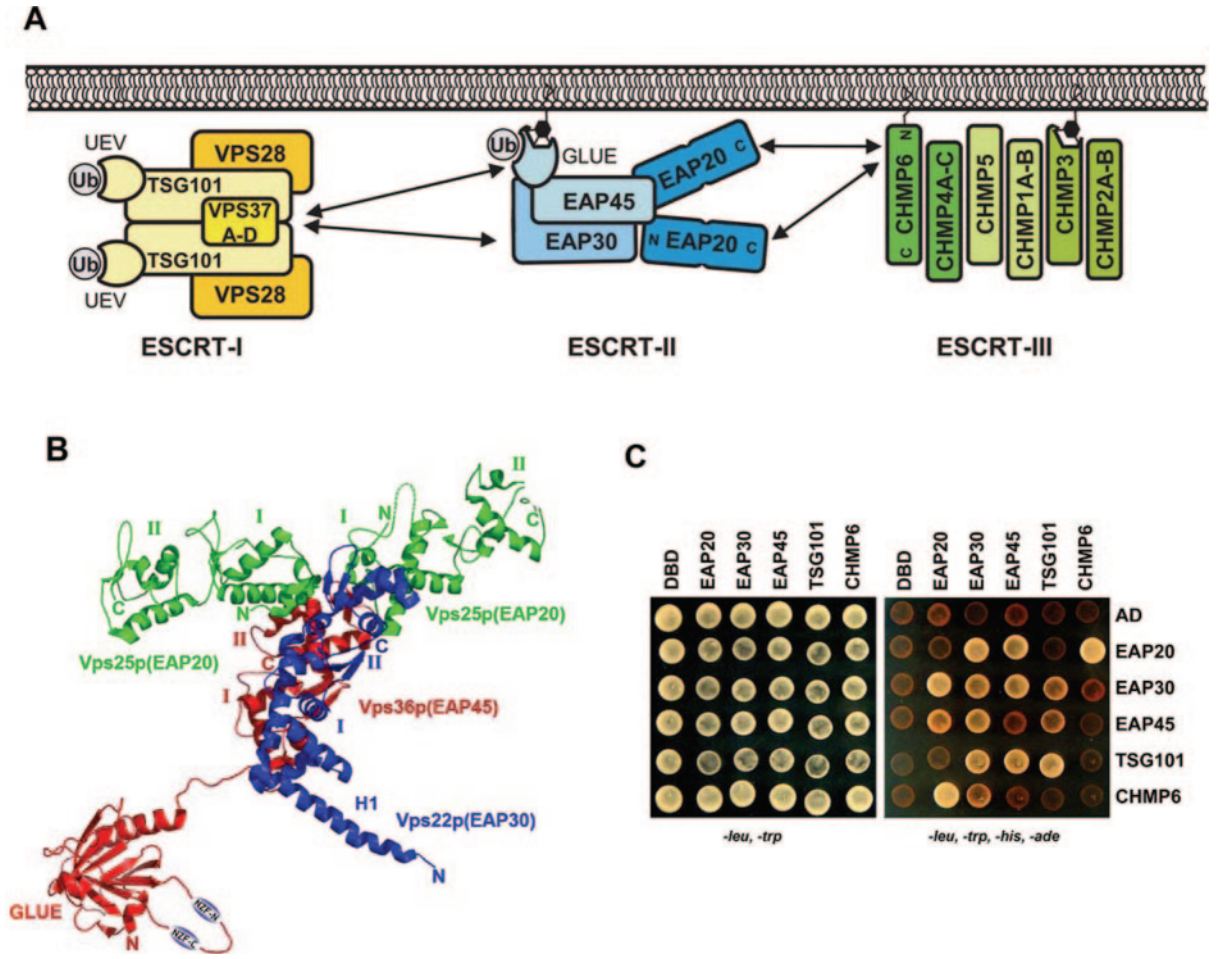

FIG. 1. ESCRT-II structure and interactions. (A) Schematic model summarizing the protein interactions of the human ESCRT-II complex (see the text for details). Note that the stoichiometries and compositions of the ESCRT-I and ESCRT-III complexes have not yet been defined unambiguously. The complexes are therefore simply shown with all possible subunits. (B) Three-dimensional structure of the yeast ESCRT-II complex. The structure of the ESCRT-II core was determined by X-ray crystallography (30, 74). The N-terminal region of Vps36 (EAP45) (shown schematically) has not yet been determined but contains two NZF domains (1) embedded within a GLUE domain (67). The structural elements/domains correspond approximately to the following residues (human homologs are in parentheses): for Vps36p (EAP45), GLUE domain, 1 to 285 (1 to 135); NZF-1, 177 to 205; NZF-2, 242 to 259 (neither NZF motif is present in EAP45); linker domain, 286 to 404 (136 to 238); WH-1, 405 to 491 (239 to 316); and WH-2, 492 to 566 (317 to 386); for Vps22p (EAP30), helix 1 (H1), 1 to 51 (1 to 55); WH-1, 90 to 165 (95 to 176); and WH-2, 166 to 233 (177 to 258); for Vps25p (EAP20), WH-1, 19 to 127 (22 to 103), and WH-2, 128 to 200 (104 to 176). (C) Summary of the positive yeast two-hybrid interactions between ESCRT-II proteins and all known human class E proteins. The right array shows doubly transformed yeast replica plated on minus Leu, minus Trp, minus His, minus Ade selection media, where successful growth represents a positive protein interaction. The left array shows replica-plated yeast on minus Leu, minus Trp media (a control for equivalent transformation and yeast growth). The indicated constructs were fused to DBDs (rows) or ADs (columns). Unfused DBD and AD constructs are shown as negative controls. Note that the interaction between DBD-EAP30 and AD-CHMP6 was judged to be negative because it was very weak and was not detected in the reciprocal direction. Analogous data were summarized previously in reference 83.

lated as a stable, soluble complex composed of three proteins that share 19 to 36% pairwise identity with their *S. cerevisiae* homologs (excluding the N-terminal region of Vps36p/EAP45) (37, 61). We have therefore used the crystal structure of the *S. cerevisiae* ESCRT-II core as a working model for the human ESCRT-II complex (Fig. 1B) (see Materials and Methods). Mammalian ESCRT-II functions are less well studied than those of the yeast complex, but the mammalian EAP20 and EAP45 proteins do colocalize with ESCRT-III components and with ubiquitylated proteins on endosomal membranes (67, 88). Like their yeast counterparts, EAP20 can bind the ESCRT-III protein, CHMP6 (46, 83, 88), and the N-terminal GLUE domain of murine EAP45 was recently shown to bind ubiquitin (67). These observations all support the idea that the mammalian and *S. cerevisiae* ESCRT-II complexes are functional homologs. Nevertheless, there must also be important differences between human and yeast ESCRT-II proteins. For example, the mammalian complex lacks both NZF domains and therefore must interact differently with both ESCRT-I and ubiquitin. Moreover, ESCRT-II and CHMP6 overexpression does not inhibit HIV type 1 (HIV-1) budding (46), and it was recently reported that ESCRT-II is not required for lysosomal degradation of major histocompatibility complex I (MHC-I) or epidermal growth factor receptor (EGFR), indicating that the

complex is not absolutely required for membrane protein sorting or MVB vesicle formation (11). Indeed, several groups have proposed that ESCRT-II complexes in other species may perform functions that appear to be unrelated to MVB protein sorting. These include a role for mammalian ESCRT-II in transcriptional elongation (37, 61, 65) and a role for the *Schizosaccharomyces pombe* ESCRT-II protein EAP30 in meiotic spindle pole body amplification (35). The relationship between MVB protein sorting and these other putative ESCRT-II activities, if any, is not yet clear.

During HIV-1 assembly, human class E proteins are recruited by two short sequence motifs (termed "late domains") within the C-terminal p6 region of the Gag polyprotein (reviewed in references 15, 19, 22, 47, 48, 52, 70, and 79). The first $p6^{gag}$ late domain is a PTAP tetrapeptide motif that binds and recruits TSG101 (*t*umor *s*usceptibility *g*ene 101; yeast Vps23p). TSG101 is the central protein of the human ESCRT-I complex, and there is good evidence that the entire ESCRT-I complex functions directly in HIV-1 release (15, 19, 22, 24, 48). The second late domain within $p6^{gag}$ is a YPX_nL motif (where X_n can vary in identity and length) that binds and recruits ALIX/AIP1 (yeast Bro1p) (69, 80). ALIX functions late in MVB biogenesis (56) and binds both ESCRT-I (83) and ESCRT-III (41) proteins but is not a permanent subunit of any of the three discrete ESCRT complexes. Like TSG101, ALIX functions directly in virus release, although disruptions of the PTAP-TSG101 interaction generally inhibit HIV-1 budding to a greater degree than do disruptions of the ALIX-YPX_nL interaction (16, 46). As noted above, there are also indications that HIV-1 budding requires the activities of the late-acting ESCRT-III, LIP5, and VPS4 class E proteins (22, 46, 69, 83, 85). Specifically, HIV-1 release is dominantly inhibited by overexpression of VPS4 ATPase mutants and ESCRT-III proteins with large N- or C-terminal extensions (22, 46, 69, 83). HIV-1 release is also impaired by small interfering RNA (siRNA) depletion of the VPS4 binding protein LIP5 (85). It is important to note, however, that these experiments do not definitively establish a direct role for these proteins in HIV-1 budding, because the inhibitory effects could also arise from sequestration of the entire ESCRT machinery at aberrant endosomal compartments (called "class E" compartments).

In summary, HIV-1 uses the ESCRT-I complex to bud from cells and also requires the activities of downstream ESCRT-III and VPS4-LIP5 complexes. In *S. cerevisiae*, ESCRT-II physically bridges the ESCRT-I and ESCRT-III complexes and is essential for MVB protein sorting and vesicle formation (4). The mammalian ESCRT-II function appears to be more complex, however, and we therefore undertook this study with the goals of characterizing the biochemical properties of human ESCRT-II and testing its role in HIV release.

MATERIALS AND METHODS

ESCRT-II homology modeling. A working model for the human ESCRT-II core was created as follows. Protein Data Bank (PDB) coordinates from a yeast ESCRT-II crystal structure (PDB accession no. 1U5T) were utilized to create a consensus template using Swiss-PdbViewer (http://www.expasy.org/spdbv/). The human and yeast ESCRT-II sequences were then aligned within Swiss-PdbViewer, the alignment was used to thread the human sequence onto the yeast ESCRT-II template, and the model was energy minimized within Swiss-PdbViewer.

Plasmids. Genes for human EAP20, EAP30, EAP45, and CHMP6 used in yeast two-hybrid and biochemical experiments were amplified from expressed sequence tag clones as described previously (83). A complete list of all constructs used in this study is provided in Table S1 in the supplemental material. Genes and fragments for yeast two-hybrid experiments were cloned into pGADT7 (activation domain) and pGBKT7 (binding domain) vectors (Clontech) using 5′ NdeI and 3′ BamHI or BglII cloning sites. Recombinant proteins used in biochemical experiments were expressed as glutathione *S*-transferase (GST) C-terminal fusions from a modified pGEX vector (GE Biosciences). This vector (pGEX2T-TEV) contained a tobacco etch virus (TEV) protease cleavage site and 5′ NdeI and 3′ BamHI or BglII cloning sites following the GST gene. Expression constructs for deletion mutants were created by amplifying and subcloning the desired fragments or by introducing a stop codon using Quickchange mutagenesis (Stratagene). For mammalian expression, ESCRT genes were cloned as EcoRI-BamHI fragments into pcDNA3.1(−)MycHis in frame with the C-terminal Myc tag, and with a Kozak sequence, ACC, inserted between the EcoRI site and the ATG start codon.

Preparation of recombinant EAP20. GST-EAP20 was expressed in *Escherichia coli* BL21(DE3) transformed with WISP05-68 (see Table S1 in the supplemental material) by induction in mid-log phase (0.4 mM IPTG [isopropyl-β-D-thiogalactopyranoside]) and allowing the protein to accumulate for 4 hours at 23°C. The cells were lysed by lysozyme treatment (2.5 mg/ml) in 50 mM Tris, pH 8.0, 300 mM NaCl, 10% glycerol, 1 mM dithiothreitol (DTT), followed by sonication and centrifugation (at 27,000 × *g* for 45 min) to remove cell debris. Soluble GST-EAP20 was bound to a glutathione-Sepharose affinity matrix (GSTPrep FF; GE Healthcare), washed, and eluted with a step gradient of 20 mM glutathione. Protein fractions were dialyzed into 25 mM Tris (pH 8.0), 150 mM NaCl, and 1 mM DTT), and the fusion protein was cleaved during dialysis with 1 mg TEV protease per 100 mg protein (24 h; 23°C). The TEV cleavage reaction mixture was adjusted to 25 mM Tris (pH 8.0), 300 mM NaCl, 10% glycerol, 1 mM DTT, and free EAP20 was separated from GST and GST-EAP20 by size exclusion chromatography (Superdex 200; GE Healthcare). This purification method typically yielded ~1.5 mg of pure protein per liter of starting culture.

Preparation of recombinant CHMP6 proteins. GST-CHMP6 expression, affinity purification, and TEV cleavage were carried out as described for GST-EAP20. Following TEV cleavage, free GST was removed by glutathione-Sepharose affinity chromatography. The solution was then diluted six-fold to reduce the salt in the buffer to 50 mM NaCl, and the CHMP6 protein was purified to homogeneity by anion-exchange chromatography on immobilized Q-Sepharose (GE Biosciences). CHMP6 eluted at ~400 mM NaCl from a linear gradient of 50 mM to 1 M NaCl in 25 mM Tris (pH 8.0), 10% glycerol, 1 mM DTT.

GST pull-down assays. GST and GST-CHMP6 fusion proteins were expressed in *E. coli* BL21(DE3) and induced at mid-log phase with 0.4 mM IPTG. Ten-milliliter cultures of cells expressing GST-CHMP6 were pelleted; resuspended in 2 ml of 300 mM NaCl, 0.1% NP-40, 10% glycerol, 1 mM DTT, 50 mM Tris (pH 8.0); and lysed by lysozyme treatment and sonication. Soluble GST-CHMP6 was incubated with 100 μl glutathione-Sepharose resin. Approximately 30 μM purified recombinant EAP20 was added to 2 μM (equivalent) of immobilized GST-CHMP6 and incubated for 30 min at 4°C in resuspension buffer. Unbound EAP20 was removed by washing with lysis buffer, and bound proteins were released from the resin by boiling it in sodium dodecyl sulfate-polyacrylamide gel electrophoresis (SDS-PAGE) loading buffer and were analyzed on Coomassie-stained 4 to 20% SDS-PAGE gradient gels.

Yeast two-hybrid binding assays. Directed yeast two-hybrid assays were performed using the Matchmaker GAL4 Yeast Two Hybrid 3 system (Clontech). Briefly, *Saccharomyces cerevisiae* AH-109 was cotransformed with pGADT7 or pGBKT7 cloning vector (Clontech) containing the inserts of interest. The transformed yeast colonies were grown for 3 days at 30°C on yeast extract-peptone-dextrose plates with minus Leu, minus Trp selection. Ten to 100 colonies were pooled, resuspended in a liquid culture of Sabourand dextrose broth (minus Leu, minus Trp), selected on Sabourand dextrose broth (minus Leu, minus Trp, minus Ade, minus His) plates, and allowed to grow for 3 days.

Antibody production. Antibodies against the purified recombinant proteins EAP20 (UT461 and -462) and CHMP6 (UT463 and -464) were raised in rabbits by Covance Inc., following their 87-day protocol (http://abservices.crpinc.com/ab_sampleProtocols.aspx). UT461 and UT463 were affinity purified with the respective proteins, as described previously (83).

Biosensor binding experiments. EAP45-ubiquitin biosensor binding experiments were performed at 20°C using a BIACORE 2000 (Biacore AB, Uppsala, Sweden) equipped with a research grade CM4 sensor chip. Approximately 5,000 response units (RU) anti-GST antibody was immobilized on all four flow cells using amine-coupling chemistry (36). GST-$EAP45_{1–229}$, GST-$EAP45_{1–139}$, or recombinant GST alone from soluble *E. coli* lysates was diluted in running buffer

(20 mM Tris, pH 8.0, 100 mM NaCl, 1 mM DTT, 0.2 mg/ml bovine serum albumin [BSA], and 0.005% P20) and captured on the antibody surfaces at densities of ~0.5 kRU. Pure GST alone was also captured as a blank reference. Ubiquitin was purified (84), diluted in running buffer, and injected in duplicate or triplicate over the four flow cells at concentrations of 0 to 1,250 μM. Responses were collected at a rate of 2 Hz during the 30-s association and dissociation phases. Binding isotherms from the equilibrium phases were fitted to simple 1:1 binding models to determine the dissociation constant and statistical fitting errors (see Fig. 4) (53). To obtain more accurate estimates for the dissociation constant and standard errors, the interaction between GST-EAP45$_{1–139}$ and ubiquitin was measured in six independent experiments, yielding values of 410 ± 90 μM. Biosensor binding experiments for EAP20 and GST-CHMP6 were performed as described for the EAP45-ubiquitin interaction, except that a BIACORE 3000 instrument was used and binding was examined in a buffer containing 50 mM Tris, pH 8.0, 300 mM NaCl, 10% glycerol, 1 mM DTT, 0.2 mg/ml BSA, and 0.005% P20. Anti-GST antibody was immobilized over all four flow cells (~13,000 RU/cell), and CHMP6, CHMP6$_{1–100}$, and CHMP6$_{101–200}$ were captured to densities of ~2,700 RU. Purified EAP20 was diluted in running buffer and injected in triplicate at 0.03 to 560 μM concentrations.

Immunofluorescence. COS-7 cells grown on collagen-coated glass coverslips in 12-well plates were transfected with 0.5 μg of pEGFP-VPS4A-KQ DNA and, in some experiments, 0.5 μg pcDNA3.1-EAP20-myc DNA or pcDNA3.1-EAP30-myc DNA, using 2 μl Lipofectamine 2000 (Invitrogen) following the manufacturer's instructions. The cells were fixed 24 h posttransfection in 4% paraformaldehyde-phosphate-buffered saline (PBS), blocked in 10% fetal calf serum (FCS) in PBS containing 0.1% Triton X-100, and incubated at room temperature with murine monoclonal anti-Myc (9E10; Covance Inc.) to detect transfected Myc-tagged ESCRT-II proteins or with anti-EAP20 UT461 (1:1,000) or anti-CHMP6 UT463 (1:1,000) antibody to detect endogenous ESCRT proteins. Secondary antibodies were anti-mouse Alexa 594- or anti-rabbit Alexa 594-conjugated antibodies (Molecular Probes; 1:1,000). Images of 0.5-μm-thick Z sections were collected as single wavelengths on an Olympus FV300 confocal fluorescence microscope, using Fluoview 2.0.39 software.

Viral infectivity assays. EAP20 and CHMP6 were silenced by transfecting 5 μl of 20 μM annealed siRNAs, together with 1 μg of pSL1180 (carrier DNA) and 9 μl Lipofectamine 2000, into 293T cells in six-well plates (22). The sense strands of the siRNAs were as follows (lowercase letters denote RNA, and uppercase letters denote DNA nucleotides [nt]): EAP20 (start site, nt 218), cgauccagauug uauuagaTT; CHMP6-1 (start site, nt 257), ccaugguucagaguauugaTT; and CHMP6-2 (start site, nt 284), agaucgaaaugaaagugauTT. TSG101 and INV (TSG101) siRNA constructs have been described previously (22). The levels of protein depletion were estimated by quantifying the intensities of bands in Western blots using NIH ImageJ software.

Viral-particle production was initiated during a second siRNA transfection (t = 24 h) by replacing the 1-μg carrier DNA either with an HIV-1 vector system or with an infectious R9 HIV-1 NL4-3 plasmid. Virus was harvested 24 h after the second transfection, and the titers were measured using single-cycle MAGIC assays (70). The HIV-1 vector system contained 0.38 μg pCMVΔR8.2 (54), 0.12 μg pRSV-Rev (18), 0.12 μg pMD.G (57), and 0.38 μg pWPTS-nlsLacZ (all generous gifts from D. Trono, Swiss Federal Institute of Technology). HIV-packaged *lacZ* vectors were harvested 48 h later and titered on HeLaM cells as described previously (85).

Western blotting. Viral supernatants and cellular proteins from transfected 293T cells were prepared using standard procedures (82). For Western blots, virions or cytoplasmic proteins were separated by 12% SDS-PAGE, transferred to nitrocellulose (TSG101) or polyvinylidene difluoride (all others) membranes in Tris-glycine-10% MetOH buffer, blocked in 1% (TSG101) or 5% milk, and incubated with antibodies diluted in Tris-buffered saline–0.1% Tween 20 buffer (anti-TSG101), or in 1% BSA or 5% nonfat milk in Tris-buffered saline–0.1% Tween 20. Proteins were detected by enhanced chemiluminescence (Pierce) or by imaging Alexa 680-nm (Molecular Probes; 1:10,000) or IRDye 800-nm (Rockland; 1:20,000) secondary antibody on an Odyssey scanner (Li-Cor Inc.). The primary antibodies used were rabbit anti-HIV CA (UT415 made against purified NL4-3 CA protein and affinity-purified; 1:15,000); rabbit anti-HIV MA from Didier Trono, Swiss Institute of Technology (1:25,000); rabbit anti-EAP20 UT461 (1:1,000); rabbit anti-CHMP6 UT463 or UT464 (1:1,000); and mouse anti-TSG101 (GeneTex; 1:1,000).

EGFR degradation assays. 293T or HeLa cells were plated on duplicate six-well plates in Dulbecco's modified Eagle's medium-10% fetal bovine serum, and transfected with either oligofectamine or Lipofectamine 2000 and specific siRNAs (see above). During the second siRNA transfection (t = 24 h), 1 μg R9 HIV plasmid was added to one set of cells (to control for knockdown efficiency and viral production), together with the second aliquot of 5 μl siRNA. In this case, virus and cells were harvested 48 h later (t = 72 h) and analyzed by Western blotting and MAGIC infectivity assays. The other set of cells, used in EGFR assays, was transfected a second time with siRNA-oligofectamine alone. Twenty-four hours after the second transfection (t = 48 h), the cells were reseeded on polylysine (Sigma)-coated coverslips and the next day were incubated in serum-free medium for 18 h. The cells were then incubated in the presence of 1 μg/ml human EGF (Molecular Probes/Invitrogen) for 1 h (HeLa) or 2 h (293T cells); fixed in 3.7% formaldehyde-PBS, pH 7.2, at room temperature for 20 min; and incubated with mouse anti-human EGFR (1:100; Neomarkers) in 0.1% saponin-1% bovine serum albumin-PBS, pH 7.2, at room temperature for 60 min. The cells were washed extensively and incubated in Alexa 488-conjugated goat anti-mouse immunoglobulin G (1:750) (Molecular Probes/Invitrogen). The cells were imaged using an epifluorescence microscope with MagnaFire software or an Olympus FV300 confocal fluorescence microscope with Fluoview 2.0.3.9 software using 0.5-μm sections. The fluorescence intensities were quantified using NIH ImageJ software.

EGF-lysosome colocalization assays. HeLa cells were plated on duplicate six-well plates in Dulbecco's modified Eagle's medium-10% fetal bovine serum and transfected twice with either oligofectamine or Lipofectamine 2000 (t = 0 and t = 24 h) with the siRNA oligonucleotides listed above and with EAP20-2 (start site, nt 477; gcacaaggccgagaucaucTT). At t = 48 h, the cells were reseeded on polylysine (Sigma)-coated coverslips, and at t = 72 h, the cells were switched to serum-free media for 18 more hours while being incubated with 0.1 mg/ml Alexa 488-conjugated dextran (molecular weight, 10,000). The cells were then washed extensively in growth medium followed by a 4-h chase in dextran-free/serum-free medium, placed at 0°C, incubated with 1 μg/ml EGF-Alexa Fluor 555-streptavidin complex (Molecular Probes/Invitrogen) for 60 min, and washed extensively in growth medium. Finally, the cells were incubated for 30 min at 37°C to allow time for EGF internalization and trafficking. Fluorescent images were captured with an Olympus FV300 confocal fluorescence microscope with Fluoview 2.0.3.9 software using 0.5-μm sections and analyzed using NIH ImageJ software. Three to seven fields of cells were analyzed for each sample, and the EGF-lysosome localization was scored manually, with a positive score given to any cell showing significant colocalization of the EGF and dextran markers.

KK3-mediated MHC-1 downregulation. EAP20 and CHMP6 were silenced as described above with the addition of either 2 μg of pTRACER-K3 or pTRACER empty control plasmid transfected at 24 and 48 h. Thirty-six hours after the second transfection, 5×10^5 cells were incubated in suspension with anti-human HLA-ABC antibody (1 μg/μl; eBioscience) for 1 h at 4°C in a solution of 10% FCS in PBS. The cells were washed once with 1 ml of PBS and then incubated with phycoerythrin-labeled goat anti-mouse immunoglobulin (1 μg/μl; BD Biosciences) in 10% FCS-PBS, followed by an additional wash with PBS. The cells were pelleted by centrifugation and resuspended in 1 ml PBS, and surface HLA-ABC levels were analyzed using the FACScan system (BD Biosciences).

RESULTS

Protein interactions within the ESCRT-II complex. To survey the protein interactions of human ESCRT-II, we tested for yeast two-hybrid interactions between each of the three human ESCRT-II proteins and all known human class E proteins (83). As shown in Fig. 1C, the following positive interactions were observed: EAP20-EAP30, EAP20-EAP45, EAP20-CHMP6, EAP30-EAP30, EAP30-EAP45, EAP30-TSG101, and EAP45-TSG101 (and TSG101-TSG101). All of these interactions were positive in both directions, and none of the ESCRT-II proteins interacted with control DNA binding domain (DBD) or activation domain (AD) constructs (Fig. 1C) or with any other class E proteins (data not shown). As noted above, ESCRT-II contains two copies of EAP20 and single copies of EAP30 and EAP45. Hence, all of the expected heteromeric interactions within the human ESCRT-II complex were observed, because EAP20, EAP30, and EAP45 all interacted with one another. The absence of EAP20 and EAP45 homomeric interactions can also be rationalized, because there is only a single copy of EAP45 in the complex and the two copies of EAP20 within ESCRT-II do not contact one another directly (30, 74). The observed homomeric EAP30-EAP30 interaction was unex-

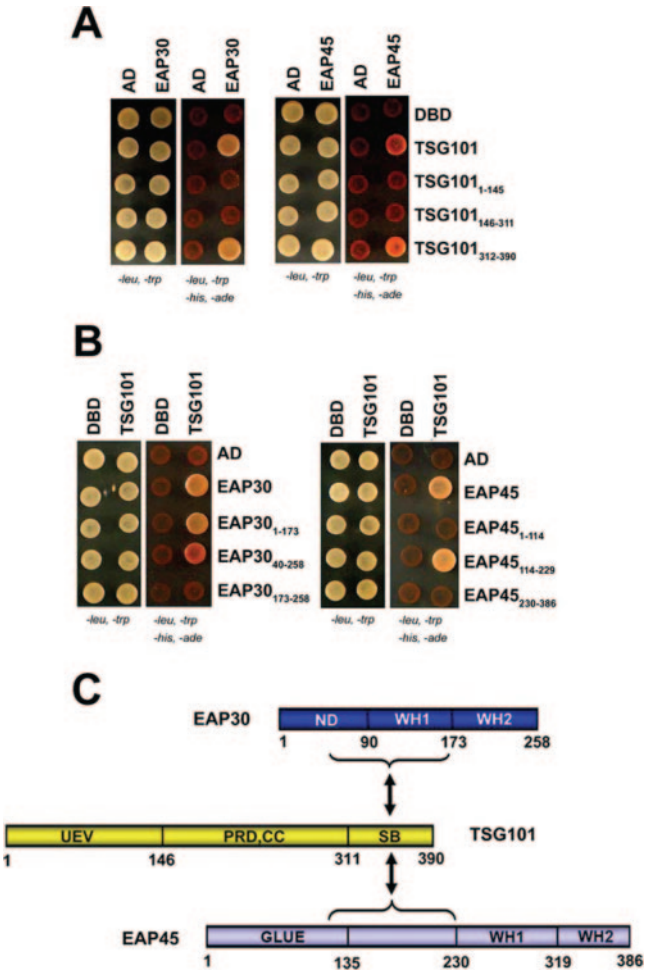

FIG. 2. Yeast two-hybrid mapping of the interaction sites between TSG101 and the EAP30 and EAP45 proteins. (A) Fragments of TSG101 binding to full-length EAP30 (left) and EAP45 (right). Selection media in the right and left arrays of each pair are the same as in Fig. 1C. (B) Full-length TSG101 binding to fragments of EAP45 (left) and EAP30 (right). (C) Schematic summary of fragment maps and interaction sites of TSG101, EAP30, and EAP45.

pected, however, and may have arisen because EAP30 was overexpressed in the absence of its other ESCRT-II binding partners. Alternatively, the interaction may reflect a natural tendency for ESCRT-II oligomerization (either directly or via bridging yeast proteins). In summary, all observed heteromeric intra-ESCRT-II interactions were consistent with structural models for the yeast and human ESCRT-II complexes, but the homomeric EAP30 interaction was not readily explained by the structure of isolated ESCRT-II.

ESCRT-I–ESCRT-II interactions. Two ESCRT-II proteins, EAP30 and EAP45, also interacted with TSG101, the central component of the ESCRT-I complex. Further mapping studies revealed that a fragment corresponding to the C-terminal region of TSG101 (termed the steadiness box [20, 42, 73]), was necessary and sufficient for both ESCRT-II protein interactions (Fig. 2A). Conversely, full-length TSG101 interacted with $EAP30_{1–173}$ and $EAP45_{114–229}$, but not with fragments outside of these regions (Fig. 2B). Thus, the TSG101 interaction site on EAP45 maps to the linker region between the GLUE domain and the first WH repeat. The TSG101 interaction site on EAP30 spans both the long N-terminal helical extension and the WH repeat. TSG101 also interacted, albeit less robustly, with an EAP30 fragment missing the first 40 amino acids that form the segment of the N-terminal helix that extends beyond the globular body of EAP30. Hence, the full EAP30 N-terminal helical extension is not strictly required for TSG101 binding, although this helix may contribute to the interaction, particularly as the full helix is predicted to extend to EAP30 residue 55.

As noted above, interactions between ESCRT-I and ESCRT-II must differ in the human and yeast systems, because the GLUE domain of human EAP45/ESCRT-II lacks the N-terminal NZF motif that forms the ESCRT-II interface in the yeast Vps28p/ESCRT-I–Vps36p/ESCRT-II complex (73). Nevertheless, we observed two-hybrid interactions for both EAP45/ESCRT-II and EAP30/ESCRT-II with human TSG101/ESCRT-I, indicating that the human ESCRT-I and ESCRT-II complexes can still interact, albeit via different ESCRT-I binding partners. Furthermore, the overall orientation of the ESCRT-I–ESCRT-II interaction may also be conserved, because the C-terminal region of TSG101 forms an extended interface with VPS28 (9, 42, 48, 73) and the TSG101 binding site on EAP45 lies immediately downstream (or at the very C-terminal end) of the GLUE domain. Thus, interactions between ESCRT-I and ESCRT-II appear to be retained in higher eukaryotes, although more detailed analyses of binding sites and energetics must await the production of pure recombinant human ESCRT complexes.

ESCRT-II–ESCRT-III interactions. In yeast, ESCRT-II recruits the downstream ESCRT-III complex through direct interactions between the ESCRT-II protein Vps25p (EAP20) and the ESCRT-III component Vps20p (CHMP6) (human homologs are in parentheses) (3, 74). Similarly, the human EAP20 and CHMP6 proteins also interacted in our two-hybrid survey of human class E proteins (Fig. 1C and 3A). Yeast two-hybrid mapping studies revealed that this interaction was mediated by the N-terminal half of CHMP6 binding to the C-terminal half of EAP20 (Fig. 3A), consistent with earlier reports (74, 88). The two C-terminal domains of EAP20 are exposed at the ends of the Y-shaped ESCRT-II complex, where they would be ideally positioned to nucleate ESCRT-III deposition through bivalent binding interactions (Fig. 1B).

GST pull-down and biosensor binding experiments with purified recombinant EAP20 and CHMP6 proteins demonstrated that the EAP20-CHMP6 interaction was direct, and these experiments again confirmed that EAP20 bound to the N-terminal half of CHMP6 (Fig. 3B and 4). As shown in Fig. 4A and B, the equilibrium binding isotherm for EAP20 binding to the full-length CHMP6 proteins fitted a simple 1:1 binding model with a dissociation constant of 5.3 ± 0.2 μM. Interestingly, EAP20 bound even more tightly to the N-terminal half of CHMP6 alone (residues 1 to 100) (equilibrium dissociation constant [K_D] = 601 ± 9 nM), and the increased affinity primarily reflected a significantly lower rate of EAP20 dissociation from the truncated CHMP6 fragment. This observation demonstrates that C-terminal sequences in CHMP6 reduce the EAP20 binding affinity, providing direct physical evidence for the proposal that isolated full-length ESCRT-III proteins can

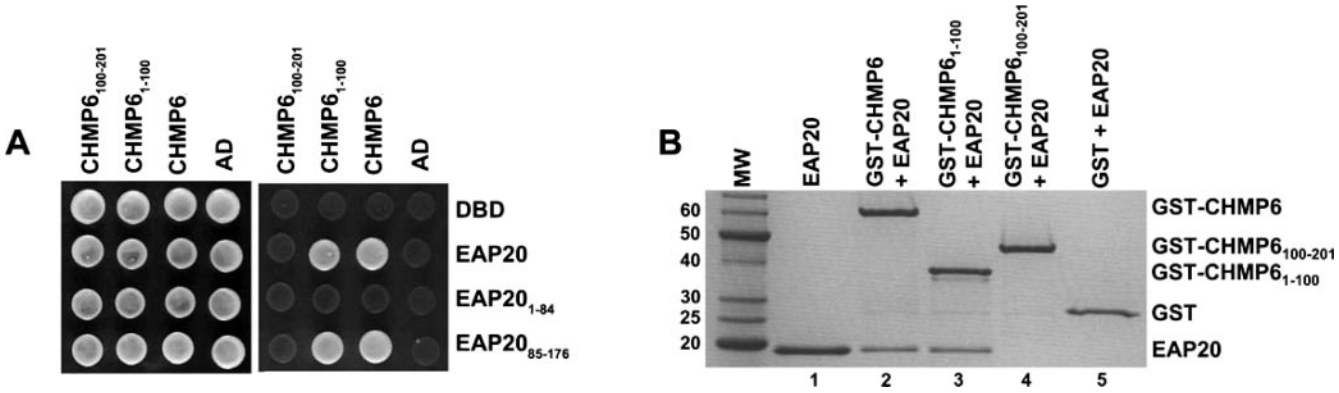

FIG. 3. Interactions between EAP20 and CHMP6. (A) Yeast two-hybrid mapping of the interaction sites between EAP20 and CHMP6. (B) GST pull-down experiment showing a direct interaction between EAP20 and the N-terminal half of CHMP6. The proteins present in each incubation mixture are given above lanes 2 to 5. Pure recombinant EAP20 is shown in lane 1 for reference. MW, molecular weight.

adopt autoinhibited "foldback" conformations (45). In this regard, it is interesting that several different CHMP proteins can be posttranslationally modified and that the unmodified CHMP proteins preferentially localize to the cytoplasm (68, 83). The posttranslational modifications might therefore destabilize autoinhibitory conformations, thereby enhancing the protein-protein interactions that help dictate ESCRT-III protein localization.

EAP45-ubiquitin interactions. The yeast ESCRT-II complex helps sort ubiquitylated protein cargoes and binds ubiquitin through the second NZF motif (NZF-C) within the N-terminal GLUE domain of Vps36p (1). Mammalian EAP45 proteins

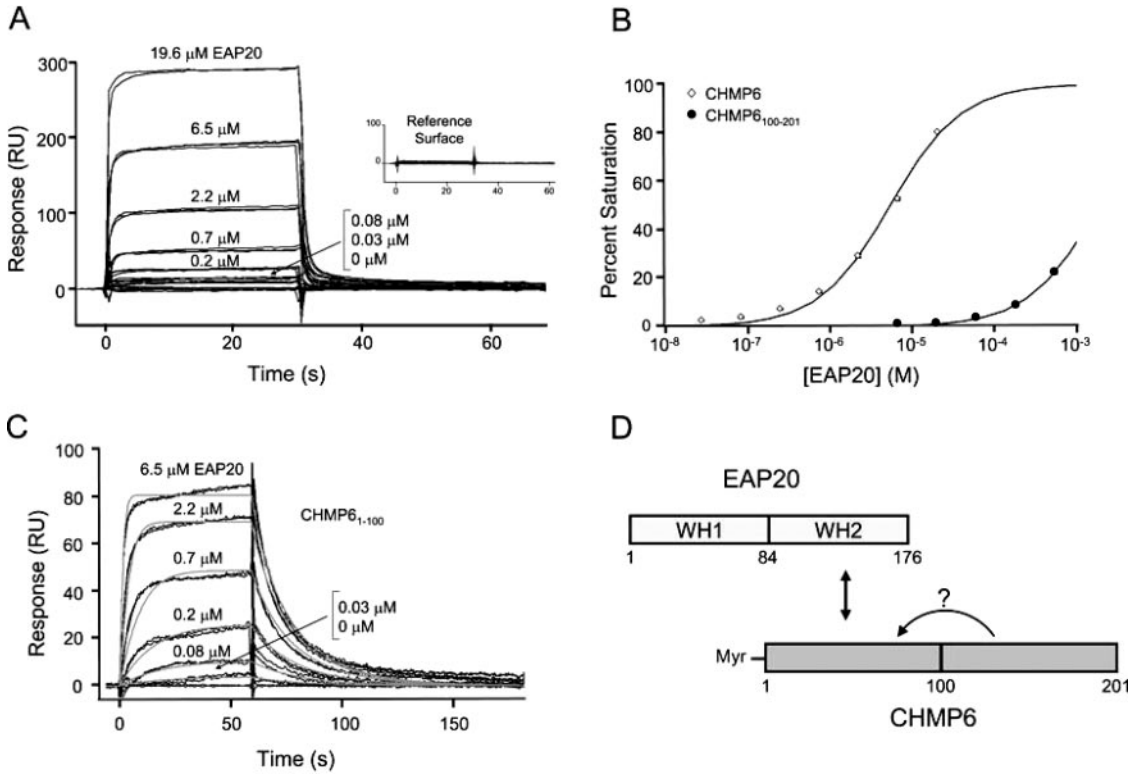

FIG. 4. Biosensor quantification of EAP20 binding to full-length and truncated CHMP6 proteins. (A) Sensorgrams showing different concentrations of EAP20 binding to full-length, immobilized GST-CHMP6. The inset shows EAP20 binding to a control GST surface. (B) Binding isotherms for EAP20 binding to full-length GST-CHMP6 ($K_D = 5.3 \pm 0.2$ μM) and GST-CHMP$_{100–201}$ ($K_D > 1$ mM). Dissociation constants and errors were derived by fitting simple 1:1 models to the equilibrium binding data (panel A and data not shown). (C) Sensorgrams showing different concentrations of EAP20 binding to GST-CHMP6$_{1–100}$. The association and dissociation phases were globally fitted to simple 1:1 interaction models. The light-gray lines show global fits with the following parameters: association rate constant $k_a = (1.46 \pm 0.04) \times 10^5$ M^{-1} s^{-1}, dissociation rate constant $k_d = 0.088 \pm 0.003$ s^{-1}, and $K_D = 601 \pm 9$ nM. (D) Schematic summary of the interaction sites between EAP20 and CHMP6. The arrow with the question mark illustrates a possible "autoinhibitory" interaction between the N- and C-terminal regions of CHMP6.

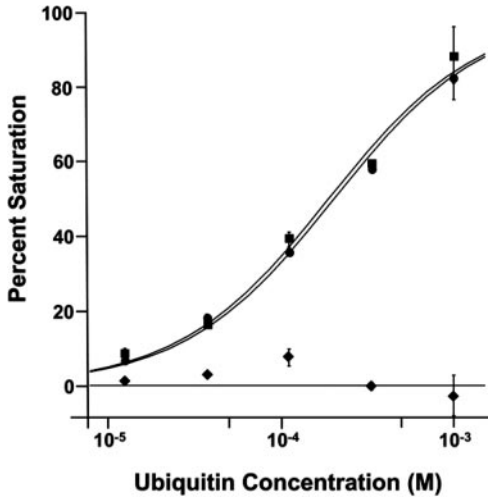

FIG. 5. Biosensor binding analyses of $EAP45_{1–229}$-ubiquitin interactions. Binding isotherms for wild-type Ub (circles) (K_D = 210 ± 10 μM), F4A Ub (squares) (K_D = 170 ± 10 μM), and I44A Ub (diamonds) (K_D > 1 mM) binding to immobilized GST-$EAP45_{1–229}$. The error bars represent standard deviations.

lack NZF motifs, however, and it has therefore been unclear whether they could still interact with ubiquitylated protein cargoes. This puzzle has recently been resolved by Slagsvold and colleagues, who showed that a minimal N-terminal fragment of murine EAP45 spanning residues 1 to 139 binds directly to ubiquitin (K_D = 460 μM) and also binds phosphoinositides (67).

We independently tested for ubiquitin binding activity in the human EAP45 protein using the entire region of human EAP45 that is missing from the crystal structure of yeast Vps36p ($EAP45_{1–229}$). Biosensor binding analyses revealed that ubiquitin bound specifically to GST-$EAP45_{1–229}$, with an estimated dissociation constant of 210 ± 10 μM in the experiment shown in Fig. 5. $EAP45_{1–229}$ binding was strongly inhibited by the Ub I44A mutation, but not by a F4A mutation, demonstrating that the exposed hydrophobic Ub I44 surface forms at least part of the EAP45 binding site. This same binding surface is also recognized by nearly all of the other ubiquitin binding proteins characterized to date (29). Ubiquitin also bound with a similar affinity to a minimal $EAP45_{1–139}$ construct (K_D = 410 ± 90 μM; n = 6), indicating that the ubiquitin binding site is located within the N-terminal GLUE domain. These data are all in excellent agreement with recent analyses of ubiquitin binding to the murine EAP45 GLUE domain (67).

EAP20 and CHMP6 accumulate on aberrant endosomal class E compartments in the absence of VPS4 ATPase activity. Under steady-state conditions, all three ESCRT complexes are predominantly cytoplasmic but assemble transiently on the endosomal membrane to participate in vesicle formation. The assembled ESCRT complexes are then recycled off the endosomal membrane by the action of the VPS4 AAA ATPases (5). Inhibition of human and yeast VPS4 ATPase activity therefore traps class E proteins, including the VPS4 proteins themselves, on aberrant endosomal class E compartments (3–5, 8, 21, 83, 89).

To test whether human ESCRT-II associated with endosomal membranes in a VPS4-dependent fashion, we examined the localization of two different ESCRT-II components, EAP20 and EAP30, in the presence of a mutant VPS4A protein (green fluorescent protein [GFP]-$VPS4A_{K173Q}$) previously shown to block ATP binding and to dominantly inhibit VPS4 activity in cells (8). As shown in Fig. 6A and B, antibodies against EAP20 detected endogenous EAP20 in COS-7 cells, albeit weakly. These antibodies also cross-reacted with a second protein of ~36 kDa (data not shown). We therefore also examined the localization of exogenous, Myc-tagged EAP20 to take advantage of the enhanced immunofluorescence signal of the tagged, overexpressed protein (Fig. 6C). In both cases, EAP20 localized to the enlarged endosomes induced by GFP-$VPS4A_{K173Q}$ overexpression. In the absence of GFP-$VPS4A_{K173Q}$, both endogenous and overexpressed EAP20 were distributed throughout the cytoplasm, as has been seen for other ESCRT complexes (Fig. 6B and D). To confirm that these results accurately represented the distribution of the entire ESCRT-II complex, the localization of a second ESCRT-II component, EAP30, was also examined. Once again, the overexpressed, Myc-tagged EAP30 protein was seen throughout the cell, but it became trapped on the class E compartments induced by dominant-negative GFP-$VPS4A_{K173Q}$ (compare Fig. 6E and F). Hence, ESCRT-II was recruited to class E compartments, where it became trapped in the absence of VPS4 ATPase activity. Localization of the endogenous ESCRT-III protein, CHMP6, was also examined, and this protein was also strongly recruited to aberrant class E compartments (Fig. 6G and H and data not shown). Similar results were obtained using the other dominant-negative ATPase constructs, GFP-$VPS4A_{E228Q}$, DsRed-$VPS4B_{K180Q}$, and DsRed-$VPS4B_{E235Q}$ (22, 83), and with human osteosarcoma cells (data not shown). These data are all consistent with the idea that human EAP20/ESCRT-II, EAP30/ESCRT-II, and CHMP6/ESCRT-III function in vesicle formation and cargo sorting at the MVB.

HIV-1 particles are released efficiently from cells depleted of EAP20. To test whether ESCRT-II is required for efficient HIV-1 budding, we measured the levels of HIV-1 vector and virus production following siRNA depletion of EAP20 or TSG101 (positive control). As shown in Fig. 7A and C, both EAP20 and TSG101 were successfully depleted to nearly undetectable levels, as determined by quantification of Western blots of cellular extracts (Fig. 7A and C, "Cells," top two rows). Importantly, intracellular Gag expression levels were not significantly altered by depletion of either protein ("Cells," bottom rows). As expected, the release of virions was dramatically reduced upon TSG101 depletion (Fig. 7A and C, "Virions," lanes "TSG101"), and the infectious titers were reduced ~20-fold (Fig. 7B and D). Surprisingly, however, depletion of EAP20 did not significantly affect viral release as measured in Western blot assays (Fig. 7A and C, "Virions", lanes "EAP20"), and actually increased vector titers slightly at the 24-h time point (Fig. 7B and D, bars 4), although at a later time point (48 h), HIV-1 titers were reduced twofold (data not shown). We therefore conclude that efficient depletion of EAP20 does not significantly inhibit the release or infectivity of HIV-1.

HIV-1 particles are also efficiently released from cells depleted of CHMP6. The efficient release of HIV-1 from EAP20-

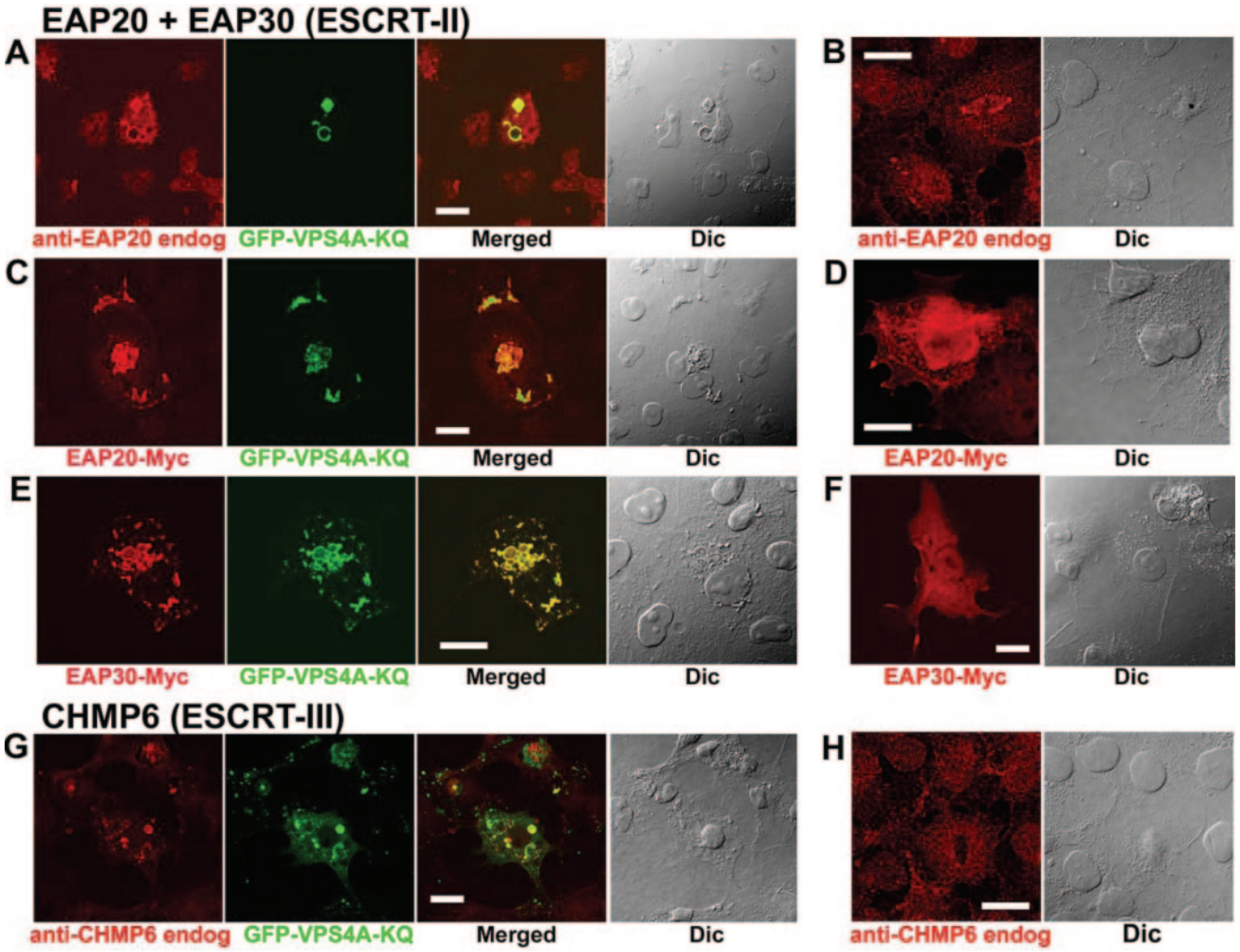

FIG. 6. Localization of ESCRT-II and ESCRT-III proteins by immunofluorescence. COS7 cells expressing fluorescent, exogenous, dominant-negative GFP-VPS4A$_{K173Q}$ (denoted GFP-VPS4A-KQ) were cotransfected and/or costained to detect the following proteins: (A) endogenous (endog) EAP20 protein (antibody UT461), (C) exogenous EAP20-Myc (anti-Myc antibody), (E) exogenous EAP30-myc (anti-Myc), and (G) endogenous CHMP6 (UT463). Column 1 (from left), ESCRT proteins alone (red); column 2, GFP-VPS4A-KQ proteins alone (green); column 3, overlaid (merged) images (colocalization on class E compartments is in yellow); column 4, differential interference contrast (Dic) images. Panels B, D, F, and H show the protein distributions in the absence of dominant-negative VPS4. Scale bars, 20 μm. Note that our two EAP20 antibodies also stained COS7 and human osteosarcoma cell centrosomes and spindles (Fig. 6B), and one of our two CHMP6 antibodies, UT 464, exhibited a punctate nuclear staining pattern in addition to staining class E membranes (not shown).

depleted cells was unexpected, and the implications of this observation were examined further by testing the requirement for CHMP6/ESCRT-III in virus release. CHMP6 was selected for study because it binds EAP20, forms the only known connection between ESCRT-II and ESCRT-III, is the only myristoylated CHMP protein (3, 88), and appears to initiate ESCRT-III assembly in yeast (3).

The effects of CHMP6 depletion on the release and infectivity of HIV-1 vectors and virus are shown in Fig. 8. As expected, virus release and infectivity were again substantially reduced upon siRNA depletion of TSG101 (Fig. 8A to D, lanes "TSG101" and bars 2), whereas treatment with an inverted control siRNA had no significant effect on virus release (defined as 100% infectivity; lanes "INV" and bars 3). Two different siRNAs were used to knock down CHMP6 (designated CHMP6-1 and CHMP6-2), and both siRNAs decreased CHMP6 levels very significantly (Fig. 8A and C, "Cells," second row) without affecting Gag protein expression or processing (third row). As with EAP20 depletion, CHMP6 depletion again failed to reduce HIV-1 release or infectivity substantially (Fig. 8A and 8C, "Virions," and B and D). Although there was some variability in multiple repetitions of this experiment, the average viral titers nevertheless fell within 40% of control levels following treatment with both CHMP6-1 and CHMP6-2 (Fig. 8B and D). At a later time point (48 h), viral infectivities were reduced four- to fivefold, possibly owing to secondary effects on general protein trafficking. We therefore conclude that normal cellular levels of CHMP6 are not required for efficient HIV-1 release or infectivity.

EAP20 and CHMP6 are required for efficient downregulation of the EGF receptor. The EGFR is normally present on the cell surface, where it can bind EGF and transmit growth

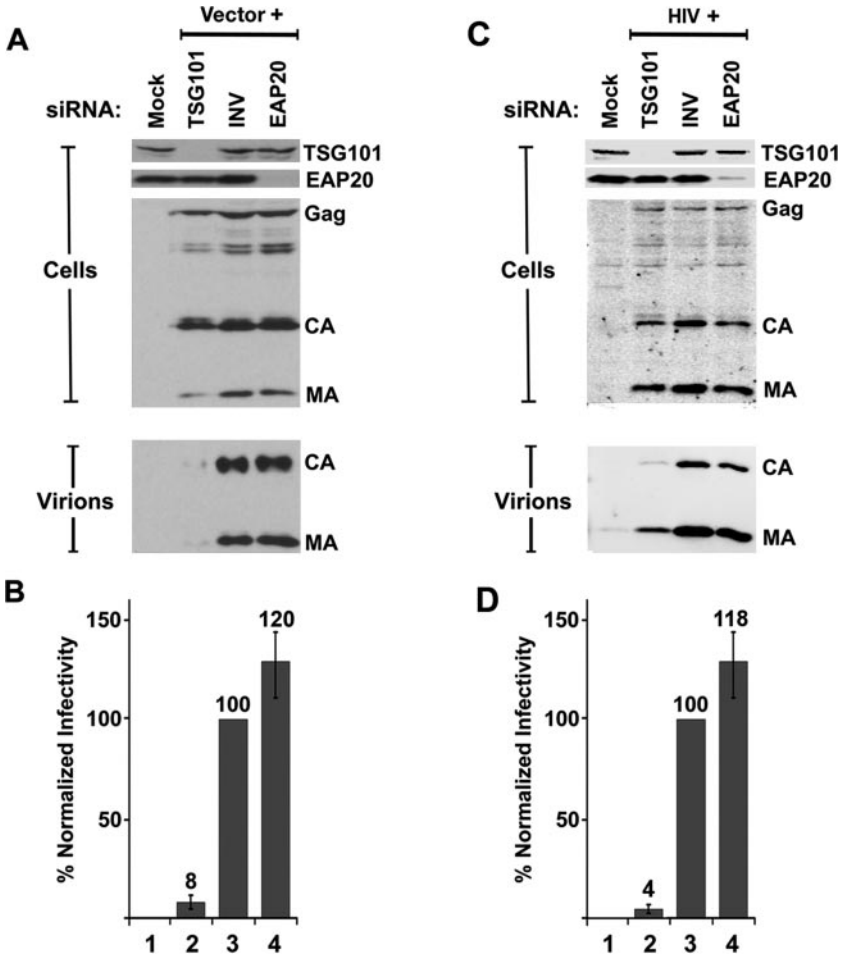

FIG. 7. siRNA depletion of EAP20 does not diminish HIV-1 vector release or transduction efficiency. (A) Western blot analysis of 293T cell extracts showing the efficiency of siRNA depletion of TSG101 (positive control, lane TSG101 in top gel) or EAP20 (lane EAP20 in second gel from top) and the effects on Gag protein expression (third gel from top) and virus-like particle release (virions, bottom gel) from a cotransfected HIV-1 vector system. Lanes Mock and INV are negative controls showing cells that were mock transfected without the HIV-1 vector or cotransfected with an inverted siRNA against TSG101 (INV), respectively. Cellular Gag, CA, and MA levels were monitored to ensure equal transfection and protein expression levels. Extracellular CA and MA levels reflect the relative efficiencies of virus-like particle release. The TSG101 signal intensity for TSG101-depleted cells was 1% of that of the control, and the EAP20 signal intensity for EAP20-depleted cells was 2% of that of the control. Quantification of at least three repetitions of this experiment showed the following levels of MA and CA release: TSG101 siRNA, 9% ± 2% of the control; inverted siRNA, 100% (defined as the control); EAP20, 108% ± 12%. The data were collected 48 h after the second siRNA transfection. (B) HIV-1 viral-vector titers produced by cells depleted of EAP20 or TSG101 (positive control). Vector transduction levels were normalized to the negative control (INV) and averaged from six independent experiments. Control vector titers were 2.5×10^5 to 3.2×10^5/ml. The data were collected 48 h after the second siRNA transfection. (C) Western blot analysis showing the efficiency and effects of siRNA-mediated silencing of EAP20 in analogous experiments with wild-type (wt) HIV-1_{NL4-3} virus. The experiment was similar to that shown in panels A and B, except that wt HIV-1_{NL4-3} virus was utilized. Quantification of at least three repetitions of this experiment showed the following levels of MA and CA release: TSG101 siRNA, 12% ± 9% of the control; inverted siRNA, 100% (defined as the control); EAP20, 75% ± 4%. The data were collected 26 h after the second siRNA transfection. (D) HIV-1 titers produced by cells depleted of EAP20 or TSG101 (positive control). Control viral titers were 0.9×10^6 to 4×10^6/ml of supernatant. The values represent the average and standard error of eight independent experiments. The data were collected 24 to 26 h after the second siRNA transfection.

signals. Following high levels of EGF stimulation, the receptor is internalized, trafficked through the MVB pathway, and degraded in the lysosome, thereby attenuating the growth signal (32, 43). The lack of a requirement for EAP20 and CHMP6 in HIV-1 budding was surprising, and we therefore tested whether depletion of these proteins altered EGFR downregulation, as would be expected for proteins that function in MVB vesicle formation and protein sorting. These experiments also served as controls for our ability to deplete TSG101, EAP20, and CHMP6 to functionally significant levels.

As shown in Fig. 9, depletion of TSG101/ESCRT-I, EAP20/ESCRT-II, and CHMP6/ESCRT-III significantly reduced the efficiency of EGFR degradation in response to EGF stimulation, although the block was not complete and was somewhat greater for TSG101/ESCRT-I than for EAP20/ESCRT-II and CHMP6/ESCRT-III. Total cellular EGFR protein levels and localization were assayed by immunofluorescence, using an anti-EGFR antibody. In the absence of EGF stimulation, EGFR was located almost exclusively on the surfaces of 293T cells (Fig. 9A, column 1 [from left] and inset). Following EGF

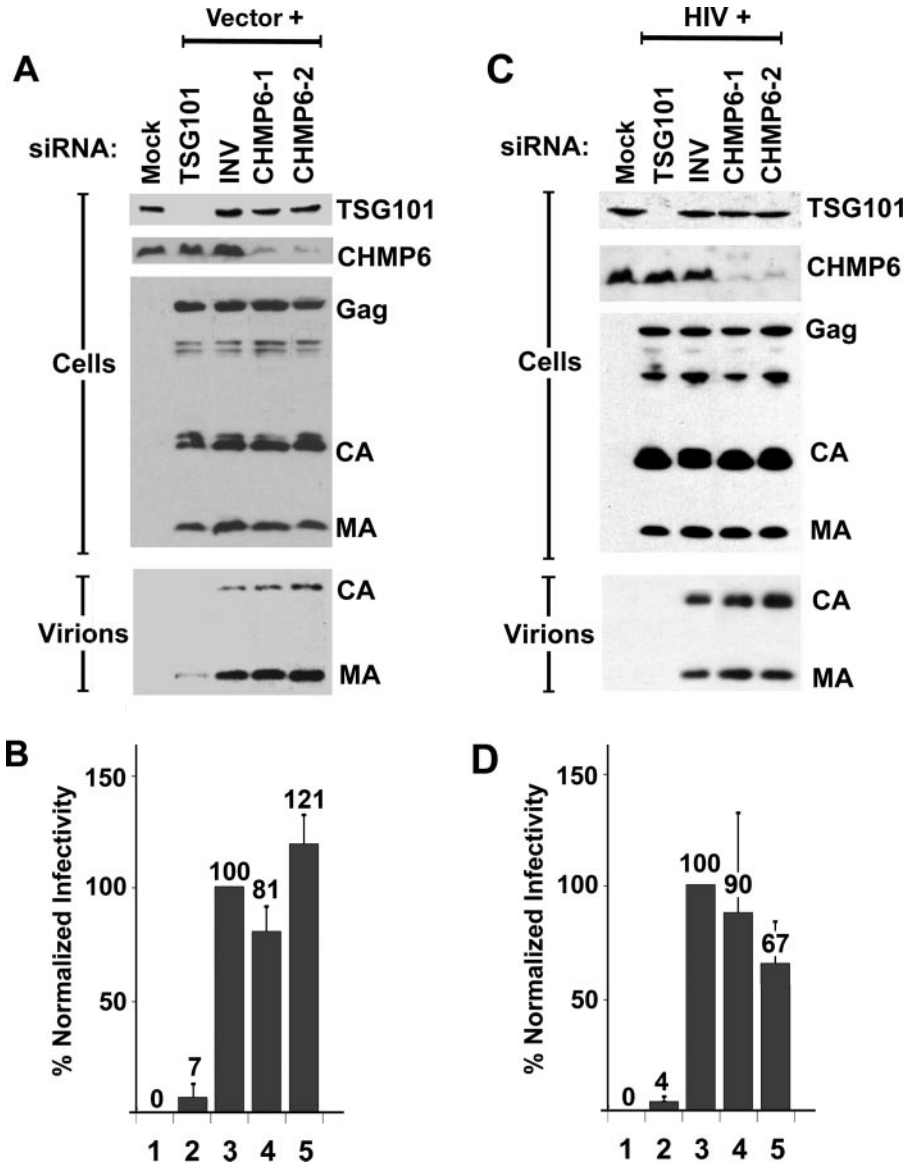

FIG. 8. HIV release and infectivity are minimally affected by CHMP6 depletion. (A) Western blot analysis of 293T cell extracts showing the efficiency of siRNA depletion of TSG101 (positive control; lane TSG101 in the top gel) or CHMP6 (lanes CHMP6-1 and -2 in the second gel from the top) and the effects on Gag protein expression (third gel from the top) and virus-like particle release (virions; bottom gel) from a cotransfected HIV-1 vector system. CHMP6 was depleted using two different siRNAs (denoted CHMP6-1 and CHMP6-2). Lanes Mock and INV are negative controls showing cells that were mock transfected without the HIV-1 vector or cotransfected with an inverted siRNA against TSG101 (INV), respectively. Cellular Gag, CA, and MA levels were monitored to ensure equal transfection and protein expression levels. The extracellular CA and MA levels reflect the relative efficiencies of virus-like particle release. The TSG101 signal intensity for TSG101-depleted cells was 2% of that of the control, and the CHMP6 signal intensities for CHMP-6-depleted cells were 12% (CHMP6-1) and 3% (CHMP6-2) relative to the control. Quantification of at least three repetitions of this experiment showed the following levels of MA and CA release: inverted siRNA, 100% (defined as the control); CHMP6-1, 133% ± 14%; and CHMP6-2, 105% ± 35%. The data were collected 48 h after the second siRNA transfection. (B) HIV-1 viral-vector titers produced by cells depleted of CHMP6 or TSG101 (positive control). Vector transduction levels were normalized to the negative control (INV) and averaged from four independent experiments. The data were collected 48 h after the second siRNA transfection. (C) Western blot analysis showing the efficiency and effects of siRNA-mediated silencing of the CHMP6 protein. The experiment was similar to that shown in panel A except that wild-type HIV-1_{NL4-3} virus was used. Quantification of at least three repetitions of this experiment showed the following levels of MA and CA release: inverted siRNA, 100% (defined as the control); CHMP6-1, 109% ± 22%; and CHMP6-2, 94% ± 38%. The data were collected 26 h after the second siRNA transfection. (D) HIV-1 titers produced by cells depleted of CHMP6 or TSG101 (positive control). Viral transduction levels were normalized to the negative control (INV) and averaged from eight independent experiments. The data were collected 26 h after the second siRNA transfection. The error bars represent standard deviations.

stimulation for 2 h, >90% of the EGFR was internalized and degraded (column 2). Importantly, EGFR degradation was significantly reduced by treatment with siRNAs against TSG101 (column 4), EAP20 (column 5), and CHMP6 (column 6), but not by treatment with a control siRNA (column 3). Depletion of the three ESCRT components did not affect receptor internalization but rather induced intracellular accumulation of internalized receptors, consistent with a defect in

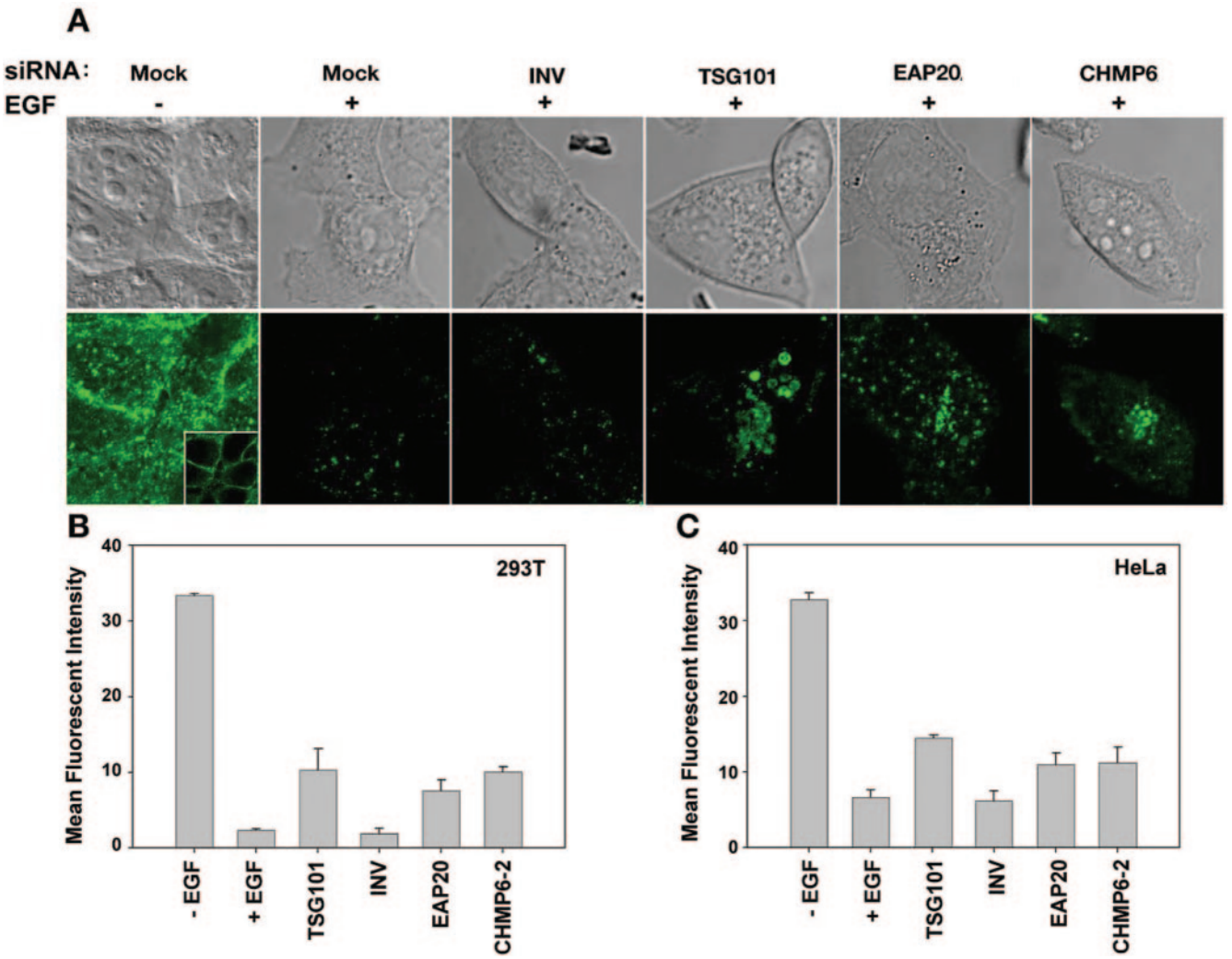

FIG. 9. EGF receptor downregulation is inhibited by depletion of TSG101, EAP20, and CHMP6. (A) 293T cells treated with siRNA were serum starved and then incubated in the presence or absence of EGF. Fixed and permeabilized cells were visualized by differential interference contrast (Nomarski) microscopy (top row) or by immunofluorescence to determine EGFR levels and localization (bottom row). Stacked whole-cell images are shown in all cases, with a central confocal slice (inset) also shown in the first image in the bottom row to demonstrate that the EGFR is located on the cell surface prior to EGF stimulation. (B) Quantification of the total levels of EGFR in 293T cells under the different conditions described for panel A. Each bar in the histogram represents the average fluorescence of individual cells as measured in three different images containing two to five cells per image. The error bars show the standard errors of the mean. The data were collected 91 h after the second siRNA transfection. (C) Quantification of total levels of EGFR in HeLa cells under the conditions described for panel A. The data were collected 92 h after the second siRNA transfection.

MVB trafficking. We note that treatment with siRNAs against TSG101 resulted in the accumulation of EGFR in larger class E compartments (17) than were seen in cells treated with siRNAs against EAP20 or CHMP6. The EGFR trafficking defects seen in the absence of ESCRT activities were similar in 293T and HeLa cells, as shown quantitatively in Fig. 9B and C. The efficiencies of protein depletion and virus release were monitored in parallel experiments that confirmed that the targeted proteins were depleted as expected and that HIV-1 release was significantly reduced by TSG101 depletion, but not by depletion of EAP20 or CHMP6 (data not shown).

Bowers et al. recently reported that siRNA depletion of EAP20 did not measurably inhibit the lysosomal degradation of MHC-I and EGF-EGFR complexes (11). This differs from our conclusion that EAP20 depletion reduced the efficiency of EGFR degradation, and we therefore investigated the issue further by testing the effects of depleting TSG101/ESCRT-I, EAP20/ESCRT-II, and CHMP6/ESCRT-III on (i) MHC-I degradation and (ii) movement of fluorescent EGF to the lysosome. In the former experiments, we found that depletion of TSG101/ESCRT-I reduced the stimulation of MHC-I receptor degradation by the Kaposi's sarcoma-associated herpesvirus ubiquitin ligase KK3 (13, 28), whereas depletion of EAP20/ESCRT-II and CHMP6/ESCRT-III did not (data not shown). These results are in excellent agreement with those of Bowers et al. (11), and we therefore conclude that efficient MHC-I downregulation requires TSG101/ESCRT-I but not EAP20/ESCRT-II or CHMP6/ESCRT-III. Thus, the ESCRT

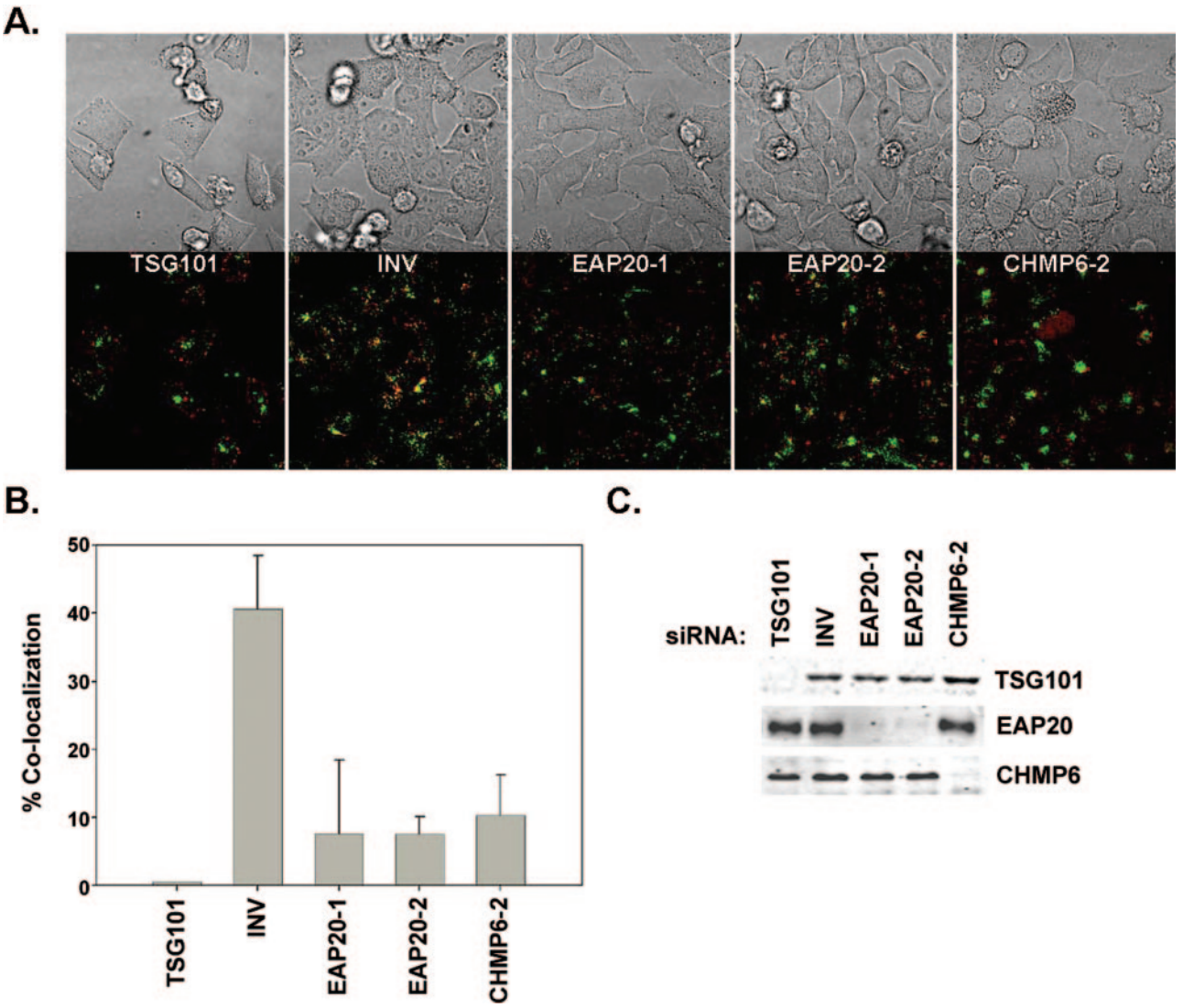

FIG. 10. Colocalization of EGF and lysosomal fluid phase markers upon depletion of TSG101, EAP20, and CHMP6. (A) HeLa cells were treated with the designated siRNA, Alexa 488-dextran (green), and EGF-Alexa Fluor 555 streptavidin (red) as described in Materials and Methods. (B) Quantification of the fractions of cells showing some colocalization of Alexa 488-dextran and EGF-Alexa Fluor 555 streptavidin under the different conditions described for panel A. The quantification of EGF (red) coincident with lysosome dextran (green) was performed in single-plane overlay analyses using the Olympus Fluoview software. Cells were scored as positive if the overlap coefficient (*R*) was greater than 0.5. The error bars represent standard deviations. (C) Western blot analysis showing the efficiency of siRNA-mediated depletion of TSG101, EAP20, and CHMP6.

requirements for MHC-I downregulation are similar to the requirements for HIV-1 budding.

We examined the trafficking of EGF to the lysosome in cells depleted of TSG101/ESCRT-I, EAP20/ESCRT-II, or CHMP6/ESCRT-III. HeLa cells depleted of TSG101/ESCRT-I, EAP20/ESCRT-II, or CHMP6/ESCRT-III were incubated with the fluid phase marker Alexa 488-dextran for 18 h, followed by a 4-h chase in dextran-free medium, which allows the fluid phase marker to accumulate in lysosomes (12, 78). As shown above, the unstimulated EGFR is predominantly localized to the plasma membrane. Incubation of cells with EGF-Alexa Fluor 555 streptavidin induced the internalization of the EGFR, and after 30 min, fluorescent EGF colocalized with lysosomes in 41% of the cells examined (Fig. 10, "INV,") (86/208 cells). In contrast, cells depleted of TSG101/ESCRT-I showed no colocalization of EGF with lysosomes ("TSG101") (0/29 cells tested). Cells depleted of either EAP20/ESCRT-II or CHMP6/ESCRT-III showed intermediate phenotypes, with 7 to 10% of the cells showing EGF staining at the lysosome. To control for possible differences between different siRNA oligonucleotides, we also tested one of the siRNA oligonucleotides used to deplete EAP20 in the study by Bowers et al. This oligonucleotide (EAP20-2) also efficiently depleted EAP20 levels (Fig. 10C) and again gave an intermediate EGF localization phenotype (Fig. 10A and B, "EAP20-2") (19/258 cells positive for EAP20-2 versus 10/140 cells for EAP20-1 and 22/213 cells for CHMP6-2).

As will be reported elsewhere, we have also now found that

degradation of ferroportin, a cell surface receptor that is downregulated by hepcidin binding (55), shows a strong dependence on TSG101, EAP20, and CHMP6 (I. De Domenico, D. M. Ward, C. Langelier, M. B. Vaughn, E. Nemeth, W. I. Sundquist, T. Ganz, G. Musci, and J. Kaplan, unpublished data). We therefore conclude that lysosomal targeting of different cell surface receptors can differ in EAP20 and CHMP6 requirements. Some receptors, such as MHC-I, exhibit little or no requirement for these proteins, while other receptors, such as ferroportin, exhibit strong requirements, and still others, such as EGFR, exhibit intermediate phenotypes. These experiments indicate that there are probably multiple pathways for sorting membrane proteins into the MVB vesicles of mammalian cells.

DISCUSSION

Not surprisingly, our studies have revealed that the human ESCRT-II complex has a number of features in common with its better-characterized yeast counterpart. The similarities include interactions with ESCRT-I, ESCRT-III, and ubiquitin; transient association with endosomal membranes; and functional participation in receptor downregulation. These observations are all consistent with the idea that ESCRT-II can play a central role in the human ESCRT pathway, interacting with the upstream ESCRT-I and downstream ESCRT-III complexes and with ubiquitylated cargos as they are sorted into MVB vesicles. Nevertheless, depletion of EAP20/ESCRT-II and CHMP6/ESCRT-III did not significantly reduce HIV-1 release from cultured 293T or HeLa cells, indicating that only a subset of the mammalian ESCRT machinery is required for efficient virus release from these cell types.

Role of EAP20/ESCRT-II in HIV-1 release. We considered several possible explanations for the observation that EAP20/ESCRT-II depletion does not inhibit HIV-1 release. As with all siRNA depletion experiments, it is possible that even the very low levels of EAP20 remaining after depletion were still sufficient to function in HIV-1 release (and MHC-I downregulation). While we cannot rule out this possible explanation, it seems unlikely because EAP20 was efficiently depleted in our experiments (Fig. 7 and 10), and this depletion measurably inhibited EGFR degradation and lysosomal targeting (Fig. 9 and 10). Furthermore, EAP20 depletion actually produced a slight, but reproducible, increase in HIV-1 infectivity (Fig. 7), which could be explained if the endogenous ESCRT-II complex binds and competes for other factors essential for virus budding (e.g., ESCRT-I). It is also conceivable that ESCRT-II may remain active even without EAP20 subunits. This explanation again seems unlikely, because the two copies of EAP20 comprise half of the ESCRT-II subunits and form the only known link between ESCRT-II and ESCRT-III. Furthermore, ESCRT-II activity is blocked by deletion of EAP20/Vps25p in both *S. cerevisiae* and *Drosophila* (4, 76, 77). We therefore conclude that the most likely explanation for our data is that ESCRT-II is not required for efficient HIV-1 release from human cells, either because the complex does not normally participate in virus budding or because the viral budding machinery still functions efficiently in its absence.

Our results also imply that if HIV-1 utilizes the late-acting ESCRT-III and VPS4 complexes to bud from cells, then there must be other proteins or complexes, in addition to ESCRT-II, that can bridge ESCRT-I and ESCRT-III. In principle, ALIX/AIP1 could be one such bridging protein, as it can bind directly to both TSG101 (83) and to the CHMP4 proteins (38, 41, 69, 83), although simultaneous depletion of ALIX and EAP20 did not synergistically inhibit EGFR degradation (11). Similarly, interactions between the yeast ESCRT-I components, Vps37p and Vps28p, and the ESCRT-III component, Vps20p (CHMP6), have been reported (10), although we did not observe analogous ESCRT-I–ESCRT-III interactions between the isolated human proteins in two-hybrid experiments. Finally, the deubiquitylating enzyme, AMSH, binds both the upstream HRS-STAM complex (which binds to TSG101) (71) and the ESCRT-III components CHMP3 and CHMP4 (23). In principle, these (and other) bridging interactions could help to recruit ESCRT-III to sites of MVB vesicle formation and virus budding even in the absence of ESCRT-II.

Role of ESCRT-III in HIV-1 release. Models for the roles of ESCRT-III (and VPS4) in virus budding must take into account the observation that HIV-1 release is not significantly inhibited by depletion of endogenous CHMP5 and CHMP6 (reference 85 and this work), yet virus release is very potently inhibited by overexpression of dominant-negative CHMP5 or CHMP6 protein (46, 69, 70). siRNA depletion of these individual CHMP proteins therefore imposes a less severe (or less general) block in the ESCRT pathway than the dominant-negative ESCRT-III and VPS4 constructs. A likely explanation for this difference is that dominant-negative CHMP (and VPS4) constructs function by inducing the formation of aberrant endosomal compartments (class E compartments) that not only inhibit the functions of the modified CHMP proteins themselves, but also sequester other ESCRT complexes and possibly many other MVB proteins required for HIV-1 budding. Thus, we cannot rule out the possibility that wild-type CHMP and VPS4 proteins do not normally function in HIV-1 release but rather affect virus budding only when present in dominant-negative forms. However, we favor a model in which at least a subset of the ESCRT-III and VPS4 proteins do actually participate directly in virus release but where depletion of individual CHMP5 or CHMP6 proteins does not inhibit virus budding owing to (i) functional redundancy within the MVB pathway arising from the presence of 10 different CHMP proteins, (ii) the possibility that CHMP5 (and possibly other CHMP proteins) may function at a step following MVB vesicle formation (7, 66), and/or (iii) the presence of multiple distinct ESCRT pathways in human cells. It therefore continues to be important to determine precisely which subset of different ESCRT proteins is utilized directly by HIV-1 and other viruses.

Complexity of MVB vesicle formation and protein sorting in higher eukaryotes. Genetic studies have identified the basic machinery required for MVB vesicle formation and protein sorting in *S. cerevisiae*. Importantly, deletion of each of the six known yeast ESCRT-I and ESCRT-II subunits ultimately leads to a strong block in protein sorting and MVB vesicle formation (the class E phenotype) (40). While it seems almost certain that the basic mechanism of MVB biogenesis is highly conserved, because human cells have at least one ortholog of every known yeast class E protein (33, 51), our studies add to the growing number of indications that MVB protein-sorting/vesicle formation pathways are more complex in higher eu-

karyotes than in yeast. One level of increased complexity is suggested by the fact that unique yeast class E proteins often have multiple orthologs in mammalian cells. Examples include the 4 different human homologs of the single yeast Vps37p protein (6, 19, 70), the 10 different human homologs of the six yeast ESCRT-III proteins (51), and the 2 (or more) different human homologs of yeast Vps4p (60). Thus, unique proteins or complexes that are essential for MVB formation in yeast may play redundant or overlapping roles in higher eukaryotes. For example, simultaneous depletion of both VPS37B and VPS37C inhibits PTAP-dependent retrovirus budding to a greater extent than depletion of either single VPS37 paralog alone (48).

A second level of complexity is suggested by the fact that even unique ESCRT-I or ESCRT-II subunits do not appear to be required for metazoan MVB vesicle formation in all contexts. For example, a knockout of the *Drosophila* Vps28/ESCRT-I protein has only modest effects on MVB morphology and no measurable effect on the downregulation of several different cell surface receptors in vivo, even though there is only a single *vps28* gene in *Drosophila* (63). Similarly, agonist-induced lysosomal degradation of the delta opioid receptor is inhibited by dominant-negative VPS4B mutants and by depletion of HRS, but not by depletion of TSG101/ESCRT-I (31). Hence, an intact ESCRT-I complex is apparently not required for downregulation of all cell surface receptors via the MVB pathway (27, 31). Similarly, EAP20/ESCRT-II is not required for MHC-I receptor downregulation induced by Kaposi's sarcoma-associated herpesvirus KK3 (reference 11 and data not shown).

Retroviruses also differ in their requirements for ESCRT-I. HIV-1, which binds directly to TSG101, requires all of the known ESCRT-I components for efficient release (19, 22, 48), whereas equine infectious anemia virus and Moloney murine leukemia virus, which bud primarily via ALIX and the Nedd4 E3 ligases, respectively, exhibit little or no requirement for TSG101/ESCRT-I (22, 48, 62, 64, 72). Nevertheless, all retroviruses are inhibited by dominant-negative ESCRT-III and VPS4 proteins, suggesting a common use of these downstream factors (22, 46, 69, 83). This model is consistent with the idea that ESCRT-I and ESCRT-II may function primarily as adaptor complexes that help recruit cargoes into the pathway, whereas the ESCRT-III/VPS4 machinery functions more directly in vesicle formation. Indeed, the genomes of *Plasmodium falciparum* and *Toxoplasma gondii* reportedly lack ESCRT-I and ESCRT-II entirely but do encode ESCRT-III and VPS4 proteins and require VPS4 to create multivesicular bodies (87). Finally, we note that even the ESCRT-III/VPS4 machinery appears to be dispensable in some cases, as the melanosomal protein Pmel17 is sorted into MVB vesicles via an ESCRT-independent pathway that is also insensitive to inhibition by dominant-negative forms of VPS4 (75). The apparent diversity of MVB sorting pathways raises the intriguing possibility that viral systems may also have evolved to utilize such "noncanonical" MVB pathways to escape the cell (34).

Roles for mammalian ESCRT-I and ESCRT-II in receptor downregulation. Although ESCRT-I and ESCRT-II are not absolutely required for the efficient downregulation of all receptors or for the release of all retroviruses, both complexes clearly play very important roles in downregulating certain cell surface receptors. Indeed, a number of recent studies indicate that both ESCRT-I and ESCRT-II exhibit growth/tumor suppressor activities by virtue of their roles in cell surface receptor downregulation. For example, all three known ESCRT-I components (TSG101, VPS28, and VPS37) have now been implicated in cell growth and tumor suppression. TSG101 was initially identified in a genetic screen for genes with tumor suppressor activity, and depletion of TSG101 induces NIH 3T3 cell overproliferation in culture and metastatic tumor formation in nude mice (44). Similarly, deletion of *erupted*, the *Drosophila* TSG101 ortholog, inhibits Notch receptor degradation and activates the JAK-STAT (and possibly other) signaling pathway and thereby induces tissue overproliferation (50). Likewise, depletion of one of the four mammalian VPS37 proteins (6, 19, 70), VPS37A/HCRP-1, enhances the growth of cultured hepatocellular carcinoma BEL-7404 cells and elevates their invasive ability (86). Interestingly, VPS37A/HCRP-1 is also downregulated in some hepatocellular carcinomas. Finally, we have observed that depletion of VPS28 can relieve contact-inhibited growth in cultured 293T cells (J. Garrus, personal communication). ESCRT-II also appears to play an important role in growth receptor downregulation, as deletion of the *Drosophila vps25* gene leads to tissue overproliferation through aberrant stabilization of the Notch and DPP (and possibly other) receptors (76, 77). Similarly, we observed that depletion of EAP20 (human VPS25) reduces the degradation rates of EGFR (Fig. 9 and 10), ferroportin (De Domenico, et al., unpublished), and presumably other cell surface receptors following ligand stimulation. Thus, just as the proteasome functions to degrade soluble proteins, the mammalian ESCRT pathway, including ESCRT-II, can play a critical role in mediating both homeostatic and regulated lysosomal degradation of integral membrane proteins.

ACKNOWLEDGMENTS

This work was supported by NIH funding to C.P.H. (GM066521), J.K. (HL29622 and DK070947), and W.I.S. (AI51174).

We thank Chris Rodesch, David Myszka, and Rebecca Rich for assistance with immunofluorescence and biosensor experiments.

REFERENCES

1. **Alam, S. L., J. Sun, M. Payne, B. D. Welch, B. K. Blake, D. R. Davis, H. H. Meyer, S. D. Emr, and W. I. Sundquist.** 2004. Ubiquitin interactions of NZF zinc fingers. EMBO J. **23:**1411–1421.
2. **Babst, M.** 2005. A protein's final ESCRT. Traffic **6:**2–9.
3. **Babst, M., D. Katzmann, E. Estepa-Sabal, T. Meerloo, and S. Emr.** 2002. Escrt-III. An endosome-associated heterooligomeric protein complex required for mvb sorting. Dev. Cell **3:**271–282.
4. **Babst, M., D. Katzmann, W. Snyder, B. Wendland, and S. Emr.** 2002. Endosome-associated complex, ESCRT-II, recruits transport machinery for protein sorting at the multivesicular body. Dev. Cell **3:**283–289.
5. **Babst, M., B. Wendland, E. J. Estepa, and S. D. Emr.** 1998. The Vps4p AAA ATPase regulates membrane association of a Vps protein complex required for normal endosome function. EMBO J. **17:**2982–2993.
6. **Bache, K. G., T. Slagsvold, A. Cabezas, K. R. Rosendal, C. Raiborg, and H. Stenmark.** 2004. The growth-regulatory protein HCRP1/hVps37A is a subunit of mammalian ESCRT-I and mediates receptor downregulation. Mol. Biol. Cell **15:**4337–4346.
7. **Bache, K. G., S. Stuffers, L. Malerod, T. Slagsvold, C. Raiborg, D. Lechardeur, S. Walchli, G. L. Lukacs, A. Brech, and H. Stenmark.** 2006. The ESCRT-III subunit hVps24 is required for degradation but not silencing of the epidermal growth factor receptor. Mol. Biol. Cell **17:**2513–2523.
8. **Bishop, N., and P. Woodman.** 2000. ATPase-defective mammalian VPS4 localizes to aberrant endosomes and impairs cholesterol trafficking. Mol. Biol. Cell **11:**227–239.
9. **Bishop, N., and P. Woodman.** 2001. TSG101/mammalian VPS23 and mammalian VPS28 interact directly and are recruited to VPS4-induced endosomes. J. Biol. Chem. **276:**11735–11742.
10. **Bowers, K., J. Lottridge, S. B. Helliwell, L. M. Goldthwaite, J. P. Luzio, and**

T. H. Stevens. 2004. Protein-protein interactions of ESCRT complexes in the yeast *Saccharomyces cerevisiae*. Traffic **5:**194–210.
11. **Bowers, K., S. C. Piper, M. A. Edeling, S. R. Gray, D. J. Owen, P. J. Lehner, and J. P. Luzio.** 2006. Degradation of endocytosed epidermal growth factor and virally ubiquitinated major histocompatibility complex class I is independent of mammalian ESCRTII. J. Biol. Chem. **281:**5094–5105.
12. **Bright, N. A., B. J. Reaves, B. M. Mullock, and J. P. Luzio.** 1997. Dense core lysosomes can fuse with late endosomes and are re-formed from the resultant hybrid organelles. J. Cell Sci. **110:**2027–2040.
13. **Coscoy, L., D. J. Sanchez, and D. Ganem.** 2001. A novel class of herpesvirus-encoded membrane-bound E3 ubiquitin ligases regulates endocytosis of proteins involved in immune recognition. J. Cell Biol. **155:**1265–1273.
14. **Demirov, D. G., and E. O. Freed.** 2004. Retrovirus budding. Virus Res. **106:**87–102.
15. **Demirov, D. G., A. Ono, J. M. Orenstein, and E. O. Freed.** 2002. Overexpression of the N-terminal domain of TSG101 inhibits HIV-1 budding by blocking late domain function. Proc. Natl. Acad. Sci. USA **99:**955–960.
16. **Demirov, D. G., J. M. Orenstein, and E. O. Freed.** 2002. The late domain of human immunodeficiency virus type 1 p6 promotes virus release in a cell type-dependent manner. J. Virol. **76:**105–117.
17. **Doyotte, A., M. R. Russell, C. R. Hopkins, and P. G. Woodman.** 2005. Depletion of TSG101 forms a mammalian "Class E" compartment: a multicisternal early endosome with multiple sorting defects. J. Cell Sci. **118:** 3003–3017.
18. **Dull, T., R. Zufferrey, M. Kelly, R. J. Mandel, M. Nguyen, D. Trono, and L. Naldini.** 1998. A third-generation lentivirus vector with a conditional packaging system. J. Virol. **72:**8463–8471.
19. **Eastman, S. W., J. Martin-Serrano, W. Chung, T. Zang, and P. D. Bieniasz.** 2005. Identification of human VPS37C, a component of endosomal sorting complex required for transport-I important for viral budding. J. Biol. Chem. **280:**628–636.
20. **Feng, G. H., C. J. Lih, and S. N. Cohen.** 2000. TSG101 protein steady-state level is regulated posttranslationally by an evolutionarily conserved COOH-terminal sequence. Cancer Res **60:**1736–1741.
21. **Fujita, H., M. Yamanaka, K. Imamura, Y. Tanaka, A. Nara, T. Yoshimori, S. Yokota, and M. Himeno.** 2003. A dominant negative form of the AAA ATPase SKD1/VPS4 impairs membrane trafficking out of endosomal/lysosomal compartments: class E *vps* phenotype in mammalian cells. J. Cell Sci. **116:**401–414.
22. **Garrus, J. E., U. K. von Schwedler, O. W. Pornillos, S. G. Morham, K. H. Zavitz, H. E. Wang, D. A. Wettstein, K. M. Stray, M. Cote, R. L. Rich, D. G. Myszka, and W. I. Sundquist.** 2001. Tsg101 and the vacuolar protein sorting pathway are essential for HIV-1 budding. Cell **107:**55–65.
23. **Giot, L., J. S. Bader, C. Brouwer, A. Chaudhuri, B. Kuang, Y. Li, Y. L. Hao, C. E. Ooi, B. Godwin, E. Vitols, G. Vijayadamodar, P. Pochart, H. Machineni, M. Welsh, Y. Kong, B. Zerhusen, R. Malcolm, Z. Varrone, A. Collis, M. Minto, S. Burgess, L. McDaniel, E. Stimpson, F. Spriggs, J. Williams, K. Neurath, N. Ioime, M. Agee, E. Voss, K. Furtak, R. Renzulli, N. Aanensen, S. Carrolla, E. Bickelhaupt, Y. Lazovatsky, A. DaSilva, J. Zhong, C. A. Stanyon, R. L. Finley, Jr., K. P. White, M. Braverman, T. Jarvie, S. Gold, M. Leach, J. Knight, R. A. Shimkets, M. P. McKenna, J. Chant, and J. M. Rothberg.** 2003. A protein interaction map of *Drosophila melanogaster*. Science **302:**1727–1736.
24. **Goila-Gaur, R., D. G. Demirov, J. M. Orenstein, A. Ono, and E. O. Freed.** 2003. Defects in human immunodeficiency virus budding and endosomal sorting induced by TSG101 overexpression. J. Virol. **77:**6507–6519.
25. **Gould, S. J., A. M. Booth, and J. E. Hildreth.** 2003. The Trojan exosome hypothesis. Proc. Natl. Acad. Sci. USA **100:**10592–10597.
26. **Gruenberg, J., and H. Stenmark.** 2004. The biogenesis of multivesicular endosomes. Nat Rev. Mol. Cell. Biol. **5:**317–323.
27. **Gullapalli, A., B. L. Wolfe, C. T. Griffin, T. Magnuson, and J. Trejo.** 2006. An essential role for SNX1 in lysosomal sorting of protease-activated receptor-1: evidence for retromer-, Hrs-, and Tsg101-independent functions of sorting nexins. Mol. Biol Cell. **17:**1228–1238.
28. **Hewitt, E. W., L. Duncan, D. Mufti, J. Baker, P. G. Stevenson, and P. J. Lehner.** 2002. Ubiquitylation of MHC class I by the K3 viral protein signals internalization and TSG101-dependent degradation. EMBO J. **21:**2418–2429.
29. **Hicke, L., H. L. Schubert, and C. P. Hill.** 2005. Ubiquitin-binding domains. Nat. Rev. Mol. Cell. Biol. **6:**610–621.
30. **Hierro, A., J. Sun, A. S. Rusnak, J. Kim, G. Prag, S. D. Emr, and J. H. Hurley.** 2004. Structure of the ESCRT-II endosomal trafficking complex. Nature **431:**221–225.
31. **Hislop, J. N., A. Marley, and M. Von Zastrow.** 2004. Role of mammalian vacuolar protein-sorting proteins in endocytic trafficking of a non-ubiquitinated G protein-coupled receptor to lysosomes. J. Biol. Chem. **279:**22522–22531.
32. **Huang, F., D. Kirkpatrick, X. Jiang, S. Gygi, and A. Sorkin.** 2006. Differential regulation of EGF receptor internalization and degradation by multiubiquitination within the kinase domain. Mol. Cell. **21:**737–748.
33. **Hurley, J. H., and S. D. Emr.** 2006. The ESCRT complexes: structure and mechanism of a membrane-trafficking network. Annu. Rev. Biophys. Biomol Struct. **35:**277–298.
34. **Irie, T., J. M. Licata, J. P. McGettigan, M. J. Schnell, and R. N. Harty.** 2004. Budding of PPxY-containing rhabdoviruses is not dependent on host proteins TGS101 and VPS4A. J. Virol. **78:**2657–2665.
35. **Jin, Y., J. J. Mancuso, S. Uzawa, D. Cronembold, and W. Z. Cande.** 2005. The fission yeast homolog of the human transcription factor EAP30 blocks meiotic spindle pole body amplification. Dev. Cell. **9:**63–73.
36. **Johnsson, B., S. Lofas, and G. Lindquist.** 1991. Immobilization of proteins to a carboxymethyldextran-modified gold surface for biospecific interaction analysis in surface plasmon resonance sensors. Anal. Biochem. **198:**268–277.
37. **Kamura, T., D. Burian, H. Khalili, S. L. Schmidt, S. Sato, W. J. Liu, M. N. Conrad, R. C. Conaway, J. W. Conaway, and A. Shilatifard.** 2001. Cloning and characterization of ELL-associated proteins EAP45 and EAP20. A role for yeast EAP-like proteins in regulation of gene expression by glucose. J. Biol. Chem. **276:**16528–16533.
38. **Katoh, K., H. Shibata, H. Suzuki, A. Nara, K. Ishidoh, E. Kominami, T. Yoshimori, and M. Maki.** 2003. The ALG-2-interacting protein Alix associates with CHMP4b, a human homologue of yeast Snf7 that is involved in multivesicular body sorting. J. Biol. Chem. **278:**39104–39113.
39. **Katzmann, D. J., M. Babst, and S. D. Emr.** 2001. Ubiquitin-dependent sorting into the multivesicular body pathway requires the function of a conserved endosomal protein sorting complex, ESCRT-I. Cell **106:**145–155.
40. **Katzmann, D. J., G. Odorizzi, and S. D. Emr.** 2002. Receptor downregulation and multivesicular-body sorting. Nat Rev. Mol. Cell. Biol. **3:**893–905.
41. **Kim, J., S. Sitaraman, A. Hierro, B. M. Beach, G. Odorizzi, and J. H. Hurley.** 2005. Structural basis for endosomal targeting by the Bro1 domain. Dev. Cell. **8:**937–947.
42. **Kostelansky, M. S., J. Sun, S. Lee, J. Kim, R. Ghirlando, A. Hierro, S. D. Emr, and J. H. Hurley.** 2006. Structural and functional organization of the ESCRT-I trafficking complex. Cell **125:**113–126.
43. **Le Roy, C., and J. L. Wrana.** 2005. Clathrin- and non-clathrin-mediated endocytic regulation of cell signalling. Nat. Rev. Mol. Cell. Biol. **6:**112–126.
44. **Li, L., and S. N. Cohen.** 1996. Tsg101: a novel tumor susceptibility gene isolated by controlled homozygous functional knockout of allelic loci in mammalian cells. Cell **85:**319–329.
45. **Lin, Y., L. A. Kimpler, T. V. Naismith, J. M. Lauer, and P. I. Hanson.** 2005. Interaction of the mammalian endosomal sorting complex required for transport (ESCRT) III protein hSnf7-1 with itself, membranes, and the AAA+ ATPase SKD1. J. Biol. Chem. **280:**12799–12809.
46. **Martin-Serrano, J., A. Yaravoy, D. Perez-Caballero, and P. D. Bieniasz.** 2003. Divergent retroviral late-budding domains recruit vacuolar protein sorting factors by using alternative adaptor proteins. Proc. Natl. Acad. Sci. USA **100:**12414–12419.
47. **Martin-Serrano, J., T. Zang, and P. D. Bieniasz.** 2001. HIV-1 and Ebola virus encode small peptide motifs that recruit Tsg101 to sites of particle assembly to facilitate egress. Nat. Med. **7:**1313–1319.
48. **Martin-Serrano, J., T. Zang, and P. D. Bieniasz.** 2003. Role of ESCRT-I in retroviral budding. J. Virol. **77:**4794–4804.
49. **Meyer, H. H., Y. Wang, and G. Warren.** 2002. Direct binding of ubiquitin conjugates by the mammalian p97 adaptor complexes, p47 and Ufd1-Npl4. EMBO J. **21:**5645–5652.
50. **Moberg, K. H., S. Schelble, S. K. Burdick, and I. K. Hariharan.** 2005. Mutations in erupted, the *Drosophila* ortholog of mammalian tumor susceptibility gene 101, elicit non-cell-autonomous overgrowth. Dev. Cell. **9:**699–710.
51. **Morita, E., and W. I. Sundquist.** 2004. Retrovirus budding. Annu. Rev. Cell Dev. Biol. **20:**395–425.
52. **Myers, E. L., and J. F. Allen.** 2002. Tsg101, an inactive homologue of ubiquitin ligase e2, interacts specifically with human immunodeficiency virus type 2 Gag polyprotein and results in increased levels of ubiquitinated Gag. J. Virol. **76:**11226–11235.
53. **Myszka, D. G.** 1999. Improving biosensor analysis. J. Mol. Recognit. **12:**279–284.
54. **Naldini, L., U. Blomer, F. H. Gage, D. Trono, and I. M. Verma.** 1996. Efficient transfer, integration, and sustained long-term expression of the transgene in adult rat brains injected with a lentiviral vector. Proc. Natl. Acad. Sci. USA **93:**11382–11388.
55. **Nemeth, E., M. S. Tuttle, J. Powelson, M. B. Vaughn, A. Donovan, D. M. Ward, T. Ganz, and J. Kaplan.** 2004. Hepcidin regulates cellular iron efflux by binding to ferroportin and inducing its internalization. Science **306:**2090–2093.
56. **Nikko, E., A. M. Marini, and B. Andre.** 2003. Permease recycling and ubiquitination status reveal a particular role for Bro1 in the multivesicular body pathway. J. Biol. Chem. **278:**50732–50743.
57. **Ory, D. S., B. A. Neugeboren, and R. C. Mulligan.** 1996. A stable human-derived packaging cell line for production of high titer retrovirus/vesicular stomatitis virus G pseudotypes. Proc. Natl. Acad. Sci. USA **93:**11400–11406.
58. **Patnaik, A., V. Chau, and J. W. Wills.** 2000. Ubiquitin is part of the retrovirus budding machinery. Proc. Natl. Acad. Sci. USA **97:**13069–13074.
59. **Raymond, C. K., I. Howald-Stevenson, C. A. Vater, and T. H. Stevens.** 1992. Morphological classification of the yeast vacuolar protein sorting mutants: evidence for a prevacuolar compartment in class E *vps* mutants. Mol. Biol. Cell **3:**1389–1402.

60. **Scheuring, S., R. A. Rohricht, B. Schoning-Burkhardt, A. Beyer, S. Muller, H. F. Abts, and K. Kohrer.** 2001. Mammalian cells express two VPS4 proteins both of which are involved in intracellular protein trafficking. J. Mol. Biol. **312:**469–480.
61. **Schmidt, A. E., T. Miller, S. L. Schmidt, R. Shiekhattar, and A. Shilatifard.** 1999. Cloning and characterization of the EAP30 subunit of the ELL complex that confers derepression of transcription by RNA polymerase II. J. Biol. Chem. **274:**21981–21985.
62. **Segura-Morales, C., C. Pescia, C. Chatellard-Causse, R. Sadoul, E. Bertrand, and E. Basyuk.** 2005. Tsg101 and Alix interact with murine leukemia virus Gag and cooperate with Nedd4 ubiquitin ligases during budding. J. Biol. Chem. **280:**27004–27012.
63. **Sevrioukov, E. A., N. Moghrabi, M. Kuhn, and H. Kramer.** 2005. A mutation in dVps28 reveals a link between a subunit of the endosomal sorting complex required for transport-I complex and the actin cytoskeleton in *Drosophila*. Mol. Biol. Cell **16:**2301–2312.
64. **Shehu-Xhilaga, M., S. Ablan, D. G. Demirov, C. Chen, R. C. Montelaro, and E. O. Freed.** 2004. Late domain-dependent inhibition of equine infectious anemia virus budding. J. Virol. **78:**724–732.
65. **Shilatifard, A.** 1998. Identification and purification of the Holo-ELL complex. Evidence for the presence of ELL-associated proteins that suppress the transcriptional inhibitory activity of ELL. J. Biol. Chem. **273:**11212–11217.
66. **Shim, J. H., C. Xiao, M. S. Hayden, K. Y. Lee, E. S. Trombetta, M. Pypaert, A. Nara, T. Yoshimori, B. Wilm, H. Erdjument-Bromage, P. Tempst, B. L. Hogan, I. Mellman, and S. Ghosh.** 2006. CHMP5 is essential for late endosome function and down-regulation of receptor signaling during mouse embryogenesis. J. Cell Biol. **172:**1045–1056.
67. **Slagsvold, T., R. Aasland, S. Hirano, K. G. Bache, C. Raiborg, D. Trambaiolo, S. Wakatsuki, and H. Stenmark.** 2005. Eap45 in mammalian ESCRT-II binds ubiquitin via a phosphoinositide-interacting GLUE domain. J. Biol. Chem. **280:**19600–19606.
68. **Stauffer, D. R., T. L. Howard, T. Nyun, and S. M. Hollenberg.** 2001. CHMP1 is a novel nuclear matrix protein affecting chromatin structure and cell-cycle progression. J. Cell Sci. **114:**2383–2393.
69. **Strack, B., A. Calistri, S. Craig, E. Popova, and H. G. Gottlinger.** 2003. AIP1/ALIX is a binding partner for HIV-1 p6 and EIAV p9 functioning in virus budding. Cell **114:**689–699.
70. **Stuchell, M. D., J. E. Garrus, B. Muller, K. M. Stray, S. Ghaffarian, R. McKinnon, H. G. Krausslich, S. G. Morham, and W. I. Sundquist.** 2004. The human endosomal sorting complex required for transport (ESCRT-I) and its role in HIV-1 budding. J. Biol. Chem. **279:**36059–36071.
71. **Tanaka, N., K. Kaneko, H. Asao, H. Kasai, Y. Endo, T. Fujita, T. Takeshita, and K. Sugamura.** 1999. Possible involvement of a novel STAM-associated molecule "AMSH" in intracellular signal transduction mediated by cytokines. J. Biol. Chem. **274:**19129–19135.
72. **Tanzi, G. O., A. J. Piefer, and P. Bates.** 2003. Equine infectious anemia virus utilizes host vesicular protein sorting machinery during particle release. J. Virol. **77:**8440–8447.
73. **Teo, H., D. J. Gill, J. Sun, O. Perisic, D. B. Veprintsev, Y. Vallis, S. D. Emr, and R. L. Williams.** 2006. ESCRT-I Core and ESCRT-II GLUE domain structures reveal role for GLUE in linking to ESCRT-I and membranes. Cell **125:**99–111.
74. **Teo, H., O. Perisic, B. Gonzalez, and R. L. Williams.** 2004. ESCRT-II, an endosome-associated complex required for protein sorting: crystal structure and interactions with ESCRT-III and membranes. Dev. Cell **7:**559–569.
75. **Theos, A. C., S. T. Truschel, D. Tenza, I. Hurbain, D. C. Harper, J. F. Berson, P. C. Thomas, G. Raposo, and M. S. Marks.** 2006. A lumenal domain-dependent pathway for sorting to intralumenal vesicles of multivesicular endosomes involved in organelle morphogenesis. Dev. Cell. **10:**343–354.
76. **Thompson, B. J., J. Mathieu, H. H. Sung, E. Loeser, P. Rorth, and S. M. Cohen.** 2005. Tumor suppressor properties of the ESCRT-II complex component Vps25 in *Drosophila*. Dev. Cell **9:**711–720.
77. **Vaccari, T., and D. Bilder.** 2005. The *Drosophila* tumor suppressor Vps25 prevents nonautonomous overproliferation by regulating notch trafficking. Dev. Cell **9:**687–698.
78. **van Weert, A. W., K. W. Dunn, H. J. Gueze, F. R. Maxfield, and W. Stoorvogel.** 1995. Transport from late endosomes to lysosomes, but not sorting of integral membrane proteins in endosomes, depends on the vacuolar proton pump. J. Cell Biol. **130:**821–834.
79. **VerPlank, L., F. Bouamr, T. J. LaGrassa, B. Agresta, A. Kikonyogo, J. Leis, and C. A. Carter.** 2001. Tsg101, a homologue of ubiquitin-conjugating (E2) enzymes, binds the L domain in HIV type 1 Pr55Gag. Proc. Natl. Acad. Sci. USA **98:**7724–7729.
80. **Vincent, O., L. Rainbow, J. Tilburn, H. N. Arst, Jr., and M. A. Penalva.** 2003. YPXL/I is a protein interaction motif recognized by *Aspergillus* PalA and its human homologue, AIP1/Alix. Mol. Cell. Biol. **23:**1647–1655.
81. **Vogt, V. M.** 2000. Ubiquitin in retrovirus assembly: actor or bystander? Proc. Natl. Acad. Sci. USA **97:**12945–12947.
82. **von Schwedler, U. K., T. L. Stemmler, V. Y. Klishko, S. Li, K. H. Albertine, D. R. Davis, and W. I. Sundquist.** 1998. Proteolytic refolding of the HIV-1 capsid protein amino-terminus facilitates viral core assembly. EMBO J. **17:**1555–1568.
83. **von Schwedler, U. K., M. Stuchell, B. Muller, D. M. Ward, H. Y. Chung, E. Morita, H. E. Wang, T. Davis, G. P. He, D. M. Cimbora, A. Scott, H. G. Krausslich, J. Kaplan, S. G. Morham, and W. I. Sundquist.** 2003. The protein network of HIV budding. Cell **114:**701–713.
84. **Wang, C., L. Deng, M. Hong, G. R. Akkaraju, J. Inoue, and Z. J. Chen.** 2001. TAK1 is a ubiquitin-dependent kinase of MKK and IKK. Nature **412:**346–351.
85. **Ward, D. M., M. B. Vaughn, S. L. Shiflett, P. L. White, A. L. Pollock, J. Hill, R. Schnegelberger, W. I. Sundquist, and J. Kaplan.** 2005. The role of LIP5 and CHMP5 in multivesicular body formation and HIV-1 budding in mammalian cells. J. Biol. Chem. **280:**10548–10555.
86. **Xu, Z., L. Liang, H. Wang, T. Li, and M. Zhao.** 2003. HCRP1, a novel gene that is downregulated in hepatocellular carcinoma, encodes a growth-inhibitory protein. Biochem. Biophys. Res. Commun. **311:**1057–1066.
87. **Yang, M., I. Coppens, S. Wormsley, P. Baevova, H. C. Hoppe, and K. A. Joiner.** 2004. The *Plasmodium falciparum* Vps4 homolog mediates multivesicular body formation. J. Cell Sci. **117:**3831–3838.
88. **Yorikawa, C., H. Shibata, S. Waguri, K. Hatta, M. Horii, K. Katoh, T. Kobayashi, Y. Uchiyama, and M. Maki.** 2005. Human CHMP6, a myristoylated ESCRT-III protein, interacts directly with an ESCRT-II component EAP20 and regulates endosomal cargo sorting. Biochem. J. **387:**17–26.
89. **Yoshimori, T., F. Yamagata, A. Yamamoto, N. Mizushima, Y. Kabeya, A. Nara, I. Miwako, M. Ohashi, M. Ohsumi, and Y. Ohsumi.** 2000. The mouse SKD1, a homologue of yeast Vps4p, is required for normal endosomal trafficking and morphology in mammalian cells. Mol. Biol. Cell **11:**747–763.

Supplemental Table 1. Construct Summary

Insert	Internal Clone #	Backbone	Type	Cloning Sites	Source of Gene
EAP30	WISP03 - 223	pGBKT7	Y2H	*Nde* I, *Bgl* II	ATCC# 7482524
EAP30	WISP03 - 244	pGADT7	Y2H	*Nde* I, *Bgl* II	ATCC# 7482524
$EAP30_{1-173}$	WISP05 - 71	pGBKT7	Y2H	*Nde* I, *Bgl* II	ATCC# 7482524
$EAP30_{1-173}$	WISP05 - 72	pGADT7	Y2H	*Nde* I, *Bgl* II	ATCC# 7482524
$EAP30_{40-258}$	WISP05 - 73	pGBKT7	Y2H	*Nde* I, *Bgl* II	ATCC# 7482524
$EAP30_{40-258}$	WISP05 - 74	pGADT7	Y2H	*Nde* I, *Bgl* II	ATCC# 7482524
$EAP30_{173-258}$	WISP05 - 75	pGBKT7	Y2H	*Nde* I, *BamH* I	ATCC# 7482524
$EAP30_{173-258}$	WISP05 - 76	pGADT7	Y2H	*Nde* I, *BamH* I	ATCC# 7482524
EAP45	WISP03 - 224	pGBKT7	Y2H	*Nde* I, *Bgl* II	ATCC# 7496837
EAP45	WISP03 - 245	pGADT7	Y2H	*Nde* I, *Bgl* II	ATCC# 7496837
$EAP45_{1-114}$	WISP05 - 77	pGBKT7	Y2H	*Nde* I, *BamH* I	ATCC# 7496837
$EAP45_{1-114}$	WISP05 - 78	pGADT7	Y2H	*Nde* I, *BamH* I	ATCC# 7496837
$EAP45_{114-229}$	WISP05 - 79	pGBKT7	Y2H	*Nde* I, *BamH* I	ATCC# 7496837
$EAP45_{114-229}$	WISP05 - 80	pGADT7	Y2H	*Nde* I, *BamH* I	ATCC# 7496837
$EAP45_{230-386}$	WISP05 - 81	pGBKT7	Y2H	*Nde* I, *Bgl* II	ATCC# 7496837
$EAP45_{230-386}$	WISP05 - 82	pGADT7	Y2H	*Nde* I, *Bgl* II	ATCC# 7496837
EAP20	WISP03 - 222	pGBKT7	Y2H	*Nde* I, *BamH* I	ATCC# 5353912
EAP20	WISP03 - 243	pGADT7	Y2H	*Nde* I, *BamH* I	ATCC# 5353912
$EAP20_{1-84}$	WISP05 - 83	pGBKT7	Y2H	*Nde* I, *BamH* I	ATCC# 5353912
$EAP20_{1-84}$	WISP05 - 84	pGADT7	Y2H	*Nde* I, *BamH* I	ATCC# 5353912
$EAP20_{85-176}$	WISP05 - 85	pGBKT7	Y2H	*Nde* I, *BamH* I	ATCC# 5353912
$EAP20_{85-176}$	WISP05 - 86	pGADT7	Y2H	*Nde* I, *BamH* I	ATCC# 5353912
$CHMP6_{1-100}$	WISP05 - 87	pGBKT7	Y2H	*Nde* I, *BamH* I	ATCC# 5758482
$CHMP6_{1-100}$	WISP05 - 88	pGADT7	Y2H	*Nde* I, *BamH* I	ATCC# 5758482
$CHMP6_{100-201}$	WISP05 - 89	pGBKT7	Y2H	*Nde* I, *BamH* I	ATCC# 5758482
$CHMP6_{100-201}$	WISP05 - 90	pGADT7	Y2H	*Nde* I, *BamH* I	ATCC# 5758482
TSG101	WISP03 - 218	pGBKT7	Y2H	*Nco* I, *BamH* I	HeLa cDNA
TSG101	WISP03 - 239	pGADT7	Y2H	*Nco* I, *BamH* I	HeLa cDNA
$TSG101_{1-145}$	WISP04 - 307	pGBKT7	Y2H	*EcoR* I, *BamH* I	HeLa cDNA
$TSG101_{1-145}$	WISP04 - 308	pGADT7	Y2H	*EcoR* I, *BamH* I	HeLa cDNA
$TSG101_{146-311}$	WISP04 - 309	pGBKT7	Y2H	*EcoR* I, *BamH* I	HeLa cDNA
$TSG101_{146-311}$	WISP04 - 310	pGADT7	Y2H	*EcoR* I, *BamH* I	HeLa cDNA
$TSG101_{312-390}$	WISP04 - 311	pGBKT7	Y2H	*EcoR* I, *BamH* I	HeLa cDNA
$TSG101_{312-390}$	WISP04 - 312	pGADT7	Y2H	*EcoR* I, *BamH* I	HeLa cDNA
VPS4A-KQ	WISP01 - 112	pEGFP-C1	MEV	*EcoR* I, *BamH* I	ATCC# 81449
VPS4B-KQ	WISP02 - 26	pDsRed2-C1	MEV	*EcoR* I, *BamH* I	ATCC# 6216963
EAP20	WISP05 - 92	pcDNA3.1(-)/mycHis B	MEV	*EcoR* I, *BamH* I	ATCC# 5353912
EAP30	WISP04 - 149	pcDNA3.1(-)/mycHis B	MEV	*EcoR* I, *BamH* I	ATCC# 7482524
CHMP6	WISP04 - 152	pcDNA3.1(-)/mycHis B	MEV	*EcoR* I, *BamH* I	ATCC# 5758482
$EAP45_{1-229}$	WISP05 - 91	pGEX	EEV	*Nde* I, *BamH* I	ATCC# 7496837
EAP20	WISP05 - 68	pGEX	EEV	*Nde* I, *BamH* I	ATCC# 5353912
CHMP6	WISP02 - 90	pGEX	EEV	*Nde* I, *BamH* I	ATCC# 5758482
$CHMP6_{1-100}$	WISP05 - 69	pGEX	EEV	*Nde* I, *BamH* I	ATCC# 5758482
$CHMP6_{100-201}$	WISP05 - 70	pGEX	EEV	*Nde* I, *BamH* I	ATCC# 5758482

Y2H = Yeast Two Hybrid Cloning Vector

MEV = Mammalian Expression Vector

EEV = *E.coli* Expression Vector